Corrected 21 January 2016; see full text.

RESEARCH ARTICLE SUMMARY

BRAIN CIRCUITS

Gating of hippocampal activity, plasticity, and memory by entorhinal cortex long-range inhibition

Jayeeta Basu,* Jeffrey D. Zaremba, Stephanie K. Cheung, Frederick L. Hitti, Boris V. Zemelman, Attila Losonczy, Steven A. Siegelbaum*

INTRODUCTION: The precise association of contextual cues with a behavioral experience enables an animal to discriminate between salient (harmful or rewarding) versus neutral environments. What signaling mechanisms during learning help select specific contextual signals to be stored as long-term memories? Hippocampal CA1 pyramidal neurons integrate direct multisensory excitatory input from entorhinal cortex (EC) with indirect, mnemonic excitatory input from the upstream hippocampal CA3 area, and both pathways have been implicated in memory storage. Paired activation of the direct and indirect inputs at a precise 20-ms timing interval that matches the dynamics of the cortico-hippocampal circuit induces a long-term enhancement of the activation of CA1 neurons by their CA3 inputs (input timing–dependent plasticity or ITDP). However, EC additionally sends long-range inhibitory projections (LRIPs) to CA1, the function of which is largely unknown. Here, we explore the role of the LRIPs in regulating hippocampal synaptic activity and memory.

RATIONALE: GABAergic neurons (which release the inhibitory transmitter γ-aminobutyric acid or GABA) in medial entorhinal cortex (MEC) were recently found to send to hippocampus LRIPs that form relatively weak and sparse synapses on CA1 GABAergic interneurons. As lateral entorhinal cortex (LEC) conveys important contextual and object-related information to hippocampus, we examined whether this region also sends LRIPs to CA1. We expressed channelrhodopsin-2 (ChR2) selectively in LEC inhibitory neurons and examined the synaptic effects of LRIP photostimulation. The behavioral impact of the LRIPs was determined by selectively silencing these inputs locally in CA1 during contextual fear conditioning (CFC) and novel object recognition (NOR) tasks. We also used in vivo Ca^{2+} imaging to assess how different sensory and behavioral stimuli that typically make up a contextual experience activate the LEC LRIPs. Finally, we examined how the LRIPs influence information flow through the cortico-hippocampal circuit and contribute to ITDP.

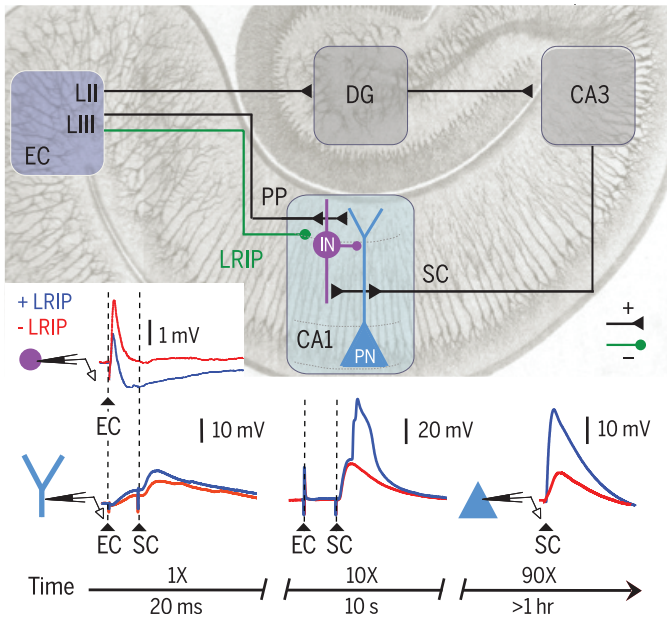

Long-range inhibitory projections gate cortico-hippocampal information flow in the short and long term. (**Top**) The cortico-hippocampal circuit. Inputs from EC arrive at CA1 directly through excitatory perforant path (PP) and LRIPs and indirectly through SCs of the trisynaptic path [dentate gyrus (DG)→CA3→CA1]. (**Bottom**) Recordings from different EC LRIP→CA1 circuit elements. (Top left) A CA1 IN that normally inhibits the pyramidal neuron (PN) dendrite is inhibited maximally by LRIP (blue, LRIP intact) 20 ms after EC stimulation (dotted guide lines). (Bottom left) This disinhibits the PN dendritic depolarization evoked by a SC input arriving 20 ms after EC input. Multiple EC-SC pairings result in more disinhibition (middle), which triggers dendritic Ca^{2+} spikes (10× pairings for 10 s) and (right) induces somatic long-term plasticity (90× pairings for 90 s) in the CA1 PN, where SC responses are potentiated for >1 hour. LRIP silencing (red) decreases dendritic depolarization and spike probability and blocks somatic plasticity. [Background from a plate by C. Golgi *et al.*, 1886; text translated and republished with plates in *Brain Res. Bull.* **54**, 461–483 (2001)]

RESULTS: LRIPs from LEC produced strong inhibitory postsynaptic potentials in a large fraction of CA1 interneurons located in the region of the EC inputs. Although pharmacogenetic silencing of LRIPs in hippocampus did not prevent CFC or NOR memory, it caused mice to show an inappropriate fear response to a neutral context and a diminished ability to distinguish a novel object from a familiar object. Calcium imaging revealed that the LRIP axons and presynaptic terminals responded to various sensory stimuli. Moreover, pairing such signals with appetitive or aversive stimuli increased LRIP activity, consistent with a role of the LRIPs in memory specificity.

ON OUR WEB SITE

Read the full article at http://dx.doi.org/10.1126/science.aaa5694

Intracellular recordings demonstrated that the LRIPs powerfully suppressed the activity of a subclass of cholecystokinin-expressing interneurons (CCK^+ INs). These interneurons were normally strongly excited by the CA3 inputs, which results in pronounced feedforward inhibition (FFI) of CA1 pyramidal neuron dendrites. By transiently and maximally suppressing the INs in a 15- to 20-ms temporal window, the LRIPs enhanced CA3 inputs onto CA1 pyramidal neurons that arrived within that timing interval. This disinhibition enabled temporally precise, paired activation of EC–Schaffer collateral (EC-SC) inputs (15 to 20 ms apart) to trigger dendritic spikes in the distal dendrites of CA1 pyramidal neurons and to induce ITDP.

CONCLUSION: LRIPs from EC act as a powerful, temporally precise disinhibitory gate of intrahippocampal information flow and enable the induction of plasticity when cortical and hippocampal inputs arrive onto CA1 pyramidal neurons at a precise 20-ms interval. We propose that the LRIPs increase the specificity of hippocampal-based long-term memory by assessing the salience of mnemonic information relayed by CA3 to the immediate sensory context conveyed by direct excitatory EC inputs. ■

The list of author affiliations is available in the full article online.
*Corresponding author. E-mail: jayeeta.basu@nyumc.org (J.B.); sas8@columbia.edu (S.A.S.)
Cite this article as J. Basu *et al.*, *Science* 351, aaa5694 (2016). DOI: 10.1126/science.aaa5694

Corrected 21 January 2016; see full text.

RESEARCH ARTICLE

BRAIN CIRCUITS

Gating of hippocampal activity, plasticity, and memory by entorhinal cortex long-range inhibition

Jayeeta Basu,[1]†‡ Jeffrey D. Zaremba,[1]* Stephanie K. Cheung,[1]*† Frederick L. Hitti,[1] Boris V. Zemelman,[2] Attila Losonczy,[1] Steven A. Siegelbaum[1]‡

The cortico-hippocampal circuit is critical for storage of associational memories. Most studies have focused on the role in memory storage of the excitatory projections from entorhinal cortex to hippocampus. However, entorhinal cortex also sends inhibitory projections, whose role in memory storage and cortico-hippocampal activity remains largely unexplored. We found that these long-range inhibitory projections enhance the specificity of contextual and object memory encoding. At the circuit level, these γ-aminobutyric acid (GABA)–releasing projections target hippocampal inhibitory neurons and thus act as a disinhibitory gate that transiently promotes the excitation of hippocampal CA1 pyramidal neurons by suppressing feedforward inhibition. This enhances the ability of CA1 pyramidal neurons to fire synaptically evoked dendritic spikes and to generate a temporally precise form of heterosynaptic plasticity. Long-range inhibition from entorhinal cortex may thus increase the precision of hippocampal-based long-term memory associations by assessing the salience of mnemonormation to the immediate sensory input.

The cortico-hippocampal circuit mediates the encoding and storage of specific associative memories, in part, through long-term plastic changes at neural circuit synapses. Most studies to date have focused on the importance of excitatory projections from entorhinal cortex (EC) to hippocampal CA1 pyramidal neurons, which provide the principal output of hippocampus (*1*–*3*). However, EC also sends long-range inhibitory projections (LRIPs) to the CA1 region of the hippocampus (*4*). At present, little is known about the role of these LRIPs in regulating hippocampal circuit operations, synaptic plasticity, or memory storage.

Excitatory glutamatergic input to the CA1 region arrives from EC through both a direct and an indirect pathway (*5*). In the indirect, or trisynaptic, path, EC LII stellate cells excite dentate gyrus granule cells, which excite CA3 pyramidal neurons. The Schaffer collateral (SC) axons of CA3 pyramidal neurons provide strong excitatory drive onto CA1 pyramidal neurons by forming synapses on CA1 apical dendrites in stratum radiatum (SR), relatively close to the soma. EC LII (*3*) and LIII (*6*) pyramidal neuron axons provide direct, but weak, excitatory drive by forming synapses on regions of the CA1 pyramidal neuron apical dendrites located in stratum lacunosum moleculare (SLM), very far from the soma. Both indirect and direct inputs also recruit strong feedforward inhibition (FFI) that normally limits CA1 excitation (*7*).

Previous studies have demonstrated that coordinated activation of the direct and trisynaptic inputs to CA1 pyramidal neurons enhances the propagation of excitatory postsynaptic potentials (EPSPs) along the pyramidal neuron apical dendrites (*8*), enables the firing of dendritic spikes and bursts of action potential output (*9*), induces a robust and temporally precise form of heterosynaptic plasticity (termed input timing–dependent plasticity or ITDP) (*10*, *11*), and leads to de novo place-cell firing (*12*). However, the contribution of the LRIPs to cortico-hippocampal activity has not been previously investigated. Here, we have characterized the activity of the LRIPs in vivo, analyzed their role in long-term memory storage, and investigated their function in regulating the effects of paired EC and CA3 input, in particular CA1 pyramidal neuron synaptic activation, dendritic spike firing, and the induction of heterosynaptic plasticity.

Lateral EC provides direct GABAergic inhibition to local CA1 interneurons

LRIPs from superficial layers of medial entorhinal cortex (MEC), an area that encodes spatial information (*13*, *14*), form synapses with inhibitory neurons (INs) located near the SR-SLM border of the CA1 region (*4*). However, the LRIPs from MEC are sparse and generate relatively weak inhibitory postsynaptic currents (IPSCs) in the CA1 INs (*4*). To determine whether lateral entorhinal cortex (LEC), which conveys multimodal nonspatial sensory information to hippocampus (*15*), sends a more potent inhibitory projection to CA1 INs, we injected recombinant Cre-dependent adeno-associated viral vectors (rAAV^{Cre}) into LEC or MEC to label the LRIPs and to achieve optogenetic control of their activity. To restrict expression to INs, viral injections were performed by using a pan γ-aminobutyric acid (GABA)–releasing or GABAergic Cre-driver mouse line [GAD2-Cre mice (*16*)] (Fig. 1A and fig. S1).

Injections of two separate rAAV^{Cre} vectors were used to express tdTomato in LEC and green fluorescent protein (GFP) in MEC. In contrast to the relatively weak and sparse inhibitory projections from MEC (*4*), LEC sent dense projections to CA1 (Fig. 1, B to E, and fig. S1) that covered twice the area in CA1 (82.05 ± 3.64%) as do the LRIPs from MEC (37.79 ± 2.35%; $P < 0.0001$, two-tailed t test, $n = 5$ mice) (fig. S2). Similar to their glutamatergic counterparts, LRIPs from MEC differentially targeted CA1 along its transverse, proximal-distal axis, with denser projections to proximal regions of CA1 (i.e., those closer to CA2) (fig. S2). In contrast to the preferential targeting of LEC excitatory inputs to distal CA1 (closer to subiculum), LRIPs from LEC were distributed fairly uniformly along the proximal-distal axis of CA1 with also a small, but significant, bias toward the proximal side (figs. S2 and S6).

To examine the functional impact of these inputs, we injected an rAAV^{Cre} vector in LEC or MEC of GAD2-Cre mice, which enabled us to express light-sensitive cation channel channelrhodopsin-2 fused with enhanced yellow fluorescent protein (ChR2-EYFP) (*17*) selectively in GABAergic neurons in either region. Photostimulation of ChR2-EYFP$^+$ GABAergic axons from LEC in the CA1 SLM region in hippocampal slices (Fig. 1C) evoked large inhibitory postsynaptic currents (IPSCs) in CA1 interneurons located in the SR/SLM border region voltage-clamped to +10 mV (139 ± 24.8 pA, n = 17 responsive cells) (Fig. 1, F and G, and fig. S3). In contrast, the amplitude of IPSCs evoked by photostimulation of ChR2-EYFP$^+$ MEC LRIPs was only one-fourth as large (37.7 ± 4.5 pA, n = 11 responsive cells; $P < 0.005$, t test) (Fig. 1, F and G). Moreover, a greater fraction of SR-SLM border INs responded to photostimulation of LEC LRIPs (53.4%) compared with MEC LRIPs (32.4%) (fig. S3B).

These synaptic currents were eliminated by GABA, types A and B ($GABA_A$ and $GABA_B$ receptor blockers 6-imino-3-(4-methoxyphenyl)-1(6*H*)-pyridazinebutanoic acid hydrobromide, SR 95531 (2 μM), and [*S*-(*R**,*R**)]-[3-[[1-(3,4-dichlorophenyl) ethyl]amino]-2-hydroxypropyl](cyclohexylmethyl) phosphinic acid, CGP 54626 (1 μM), respectively, but were unaltered by blockade of α-amino-3-hydroxy-5-methyl-4-isoxazolepropionic acid (AMPA)–type glutamate receptors [2,3-dioxo-6-nitro-1,2,3,4-tetrahydrobenzo[f]quinoxaline-7-sulfonamide, NBQX (10 μM)], which indicated that the responses represented direct IPSCs generated by GABA release from the LRIPs (Fig. 1F and fig. S3C). We failed to detect any EPSPs in CA1 SR-SLM INs when we photostimulated ChR2-YFP$^+$ LEC axons under current clamp conditions with the INs held at an initial membrane potential of −68 mV (fig. S3D), which indicated that the rAAV^{Cre} vector resulted in the selective expression of ChR2 in LEC GABAergic neurons.

[1]Department of Neuroscience, Kavli Brain Institute, Columbia University Medical Center, 1051 Riverside Drive, New York, NY 10032, USA. [2]University of Texas at Austin, Austin, TX 78712, USA. *These authors contributed equally to this work. †Present address: Department of Neuroscience and Physiology, NYU Neuroscience Institute, New York University School of Medicine, 450 East 29th Street, New York, NY 10016, USA. ‡Corresponding author. E-mail: jayeeta.basu@nyumc.org (J.B.); sas8@columbia.edu (S.A.S.)

Corrected 21 January 2016; see full text.

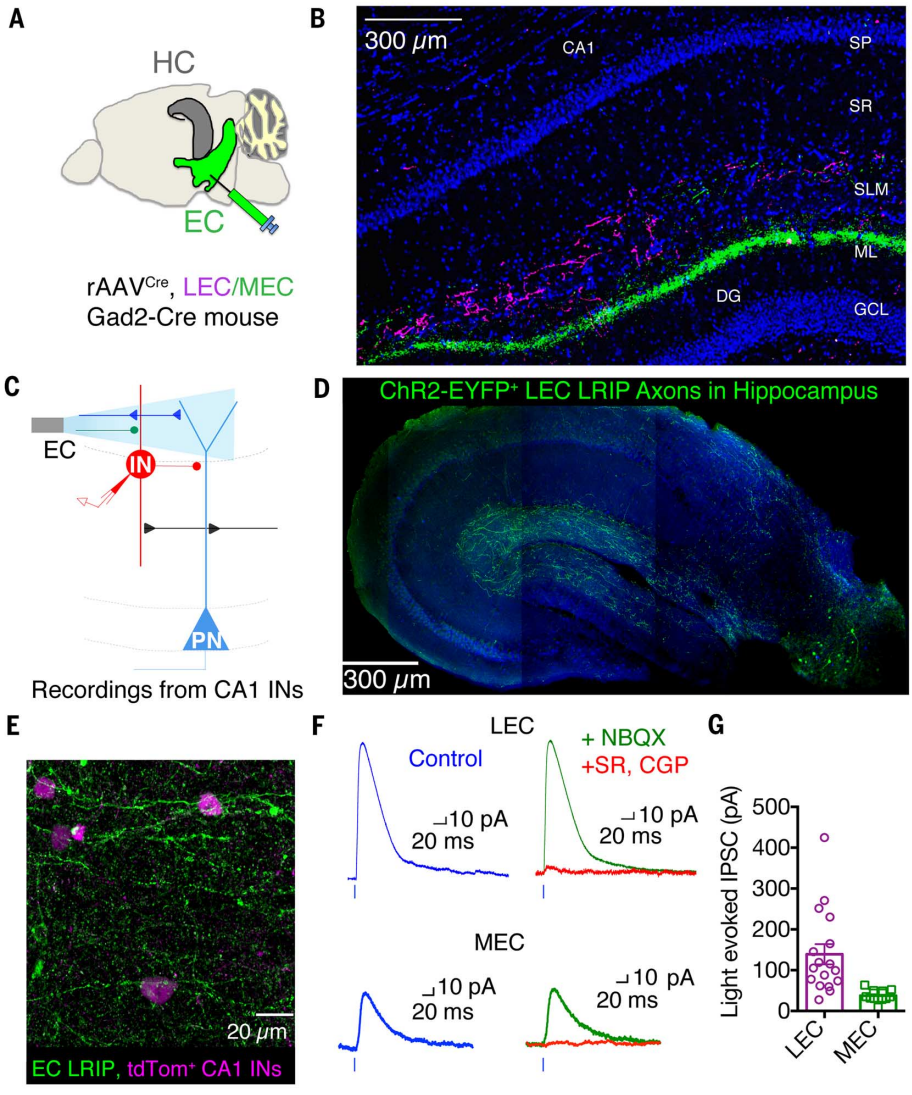

Fig. 1. LEC provides strong long-range GABAergic inputs to local CA1 inhibitory neurons. (**A**) LEC and MEC viral injection sites (in green) and their hippocampal target (HC, in gray). (**B**) TdTomato-labeled (magenta) and GFP-labeled (green) axons in SLM of CA1 from LEC and MEC Gad2-Cre^{+} LRIPs, respectively. 4′,6-diamidino-2-phenylindole (DAPI) stain in blue. The strata of hippocampal CA1 and dentate gyrus (DG): SP, stratum pyramidalis signifies pyramidal neuron (PN) cell body layer; SR, stratum radiatum where SC inputs arrive; SLM, stratum lacunosum moleculare where EC inputs arrive; and in DG, ML, molecular layer, and GCL, granule cell layer. (**C**) Scheme of experiment to functionally map impact of LRIPs from LEC or MEC on CA1 INs at SR-SLM border. ChR2-EYFP was virally expressed in GABAergic neurons in the LEC or MEC by using rAAV^{Cre} injections in *Gad2-Cre* mice. Patch-clamp recordings obtained from a CA1 IN (red) at the border of SR-SLM that targets the CA1 PN dendrite (light blue). A 470-nm laser light focused on SLM photostimulated ChR2^{+} LRIPs (green). (**D**) A 20× confocal image of ChR2-EYFP^{+} LRIP axons from LEC (green) in hippocampus from *Gad2-Cre* mouse. DAPI staining in blue. (**E**) These 63× confocal images show ChR2-EYFP^{+} LRIP axons from LEC (green) in CA1 SLM region impinging upon tdTomato^{+} IN soma (magenta). (**F**) Light-evoked IPSCs recorded from CA1 SR-SLM INs in normal extracellular solution (control, blue) and in the presence of AMPA-type glutamate receptor blocker (10 μM NBQX, green trace) or GABA receptor antagonists (2 μM SR95531 and 1 μM CGP 55845, red trace); see fig. S1 for statistics. (**G**) Bar (mean ± SEM) and scatter (individual cells) plot of the light-evoked IPSCs (pA, V_m = +10 mV) from responsive CA1 SR-SLM INs with ChR2 expressed in LEC (magenta, 139 ± 24.8 pA, n = 17) or MEC (green, 37.7 ± 4.5 pA, n = 11; P < 0.005, t test, LEC LRIP versus MEC LRIP).

LRIPs regulate the precision of memory storage

As LEC conveys nonspatial contextual information, we reasoned that the LRIP inputs may be important for nonspatial forms of learning, including contextual fear conditioning (CFC) (*18*), a hippocampus-dependent form of memory. We therefore examined the effect of silencing the LRIPs on CFC using the engineered ligand-gated glycine receptor (GlyR), PSAM (pharmacogenetically selective actuator module), which powerfully inhibits neural activity upon binding its cognate synthetic ligand PSEM^{308} (pharmacogenetically selective effector module) (*11*, *19*). To selectively silence the LEC LRIPs in CA1 without altering inhibition in EC, we implanted bilateral cannulae to locally infuse PSEM (15 μM, PSEM^{308}) in dorsal CA1 of Gad2-Cre mice expressing either GFP (control) or PSAM (test) as a result of rAAV^{Cre} injections in LEC (Fig. 2, A and B, and figs. S4 and S5). We verified that the local drug infusion selectively targeted LRIPs in hippocampus and spared EC by examining the distribution of the dye miniRuby (5%), which was present in the PSEM infusate (fig. S4, S5). PSEM^{308} infusion did not alter locomotor activity or cause anxiety-like behavior, which indicated that the drug infusion did not have significant adverse effects (fig. S7).

To test if the LRIPs were required for CFC, we infused PSEM just before the training phase on day 1 of the CFC task, in which the mice were placed in a novel context A for 2.5 min, followed by a brief, aversive foot shock (Fig. 2C) (see Materials and Methods below) (*20*). When placed in the training environment (context A) 24 hours after training (day 2, no PSEM present), the control (GFP-expressing) group demonstrated fear learning, as assessed by increased freezing behavior (Fig. 2D). However, rather than inhibiting CFC, silencing of the LEC LRIPs during training on day 1 significantly increased freezing on day 2 in context A [37.7 ± 2.3%, GFP, n = 9; 53.23 ± 2.7%, PSAM, n = 7; P < 0.0001, two-way analysis of variance (ANOVA); P < 0.001, t test, two-tailed paired by time) (Fig. 2D), which demonstrated that the LRIPs were not necessary for contextual learning.

However, when we exposed the mice on day 3 of the task to a novel context B, designed to be readily distinguishable from context A, the two groups of mice showed a revealing difference. Whereas the control mice did not freeze in the novel context, reflecting the normal specificity of CFC to the training context, the PSAM-expressing test group (where the LRIPs were only silenced during training in context A on day 1) exhibited a significant level of inappropriate freezing to the novel context (GFP: 5.1 ± 3.9%, n = 9; PSAM: 21.1 ± 7.9%, n = 7; P < 0.02, two-way ANOVA; P < 0.05, two-tailed t test paired by time) (Fig. 2D). The freezing to the novel context B in the test group was also significantly greater than the amount of freezing in context A before training (P < 0.0002), which suggested that the freezing represented an inappropriately learned response that caused an overgeneralization of fear memory. In contrast, the control group showed similar, low levels of freezing to context A on day 1 and context B on day 3 (P > 0.5). Finally, the difference in fear learning was specific for hippocampus-dependent CFC and did not reflect a general increase in fear or anxiety because the two groups of mice displayed similar extents of amygdala-dependent cued fear conditioning to a tone paired with the foot shock (Fig. 2D).

We next tested the importance of the LRIPs in a second nonspatial memory task, novel object recognition, using a version of the task that is

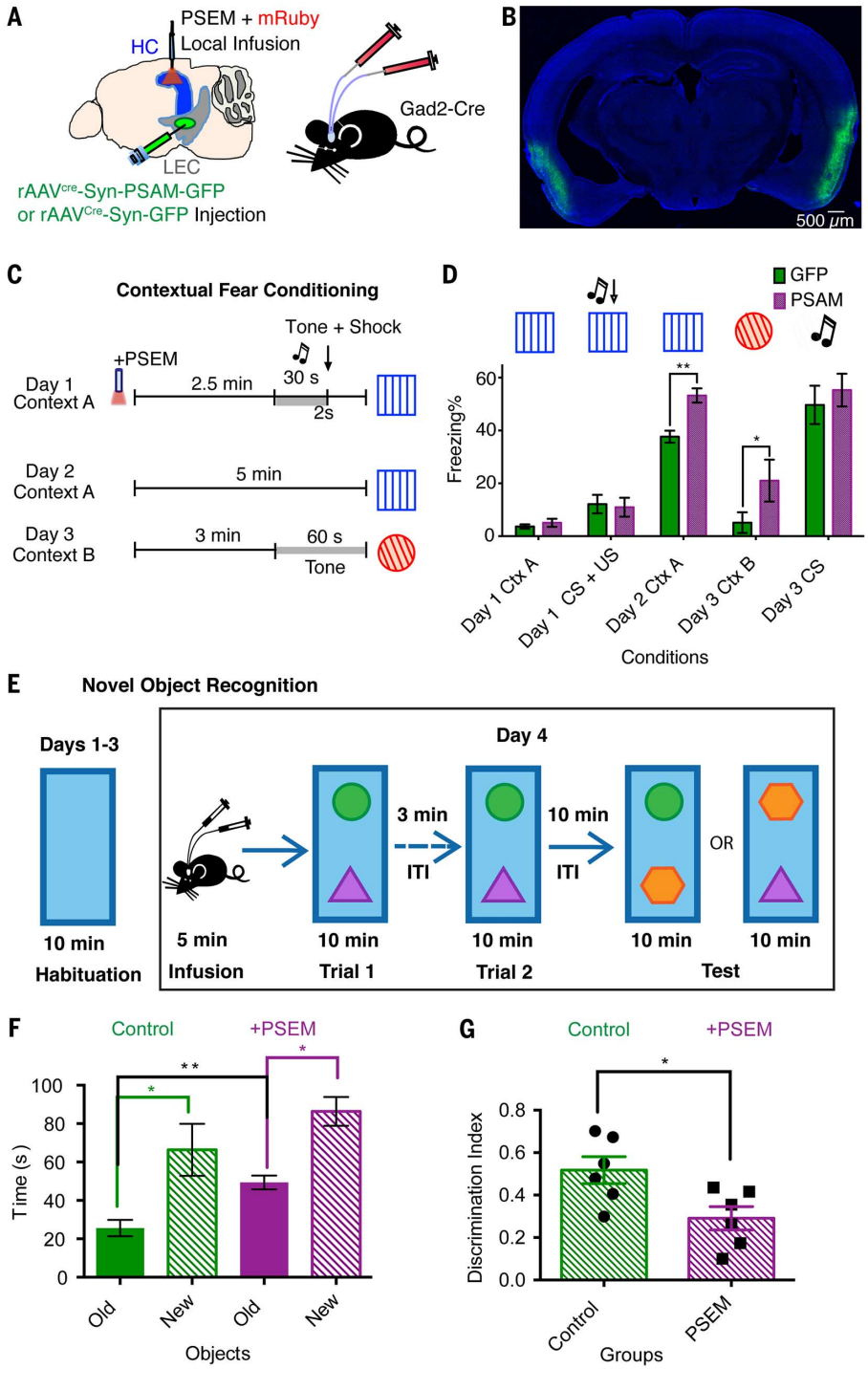

Fig. 2. Silencing LEC LRIPs in CA1 alters both context and object recognition memory. (**A**) Diagram of the experimental design. *Gad2-Cre* mice were injected with AAV^{Cre} to express GFP or PSAM in LEC. PSEM and the dye mini Ruby (mRuby) were delivered bilaterally to the CA1 region just before the training phase of memory tasks. (**B**) Confocal image (5×) of coronal section from a *Gad2-Cre* mouse injected in LEC with an AAV^{Cre}-expressing PSAM-2A-GFP, showing expression of GFP (green) in LEC (DAPI in blue). (**C**) Scheme of CFC (see Materials and Methods). On day 1, mice were exposed to context A, then given a tone followed by footshock. On day 2, mice were reexposed to context A. On day 3, mice were exposed to novel context B, followed by a tone. PSEM was delivered just before training in mice expressing GFP (control) or PSAM in LRIPs. (**D**) Bar plot (mean ± SEM) of time spent freezing (GFP, green; PSAM, purple): day 1, in context A before (Ctx A) and after (CS+US) footshock; day 2, during recall testing in context A; day 3, in novel context B before (Ctx B) and after cued tone (day 3 CS). Two-way repeated-measures ANOVA revealed no significant difference between groups in freezing on day 1 in context A (treatment × time $F_{6,105} = 0.8055$, $P = 0.5679$; treatment $F_{1,105} = 3.655$, $P = 0.0586$; time $F_{6,105} = 8.583$, $P < 0.0001$). There was significantly greater freezing in PSAM versus GFP groups in context A on day 2 (treatment × time $F_{4,48} = 0.8918$, $P = 0.4761$; treatment $F_{12,48} = 5.069$, $P < 0.0001$; time $F_{4,48} = 11.75$, $P < 0.0001$) and in context B (no tone) on day 3 (treatment × time $F_{3,45} = 1.230$, $P = 0.3069$; treatment $F_{15,45} = 2.246$, $P < 0.02$; time $F_{3,45} = 53.01$, $P < 0.0001$). The PSAM group also showed significantly greater freezing on day 3 in context B versus context A on day 1 before footshock (treatment $F_{12,24} = 5.332$; time $F_{2,24} = 19.76$; $P < 0.0002$). The GFP control group showed no significant difference in freezing in context A on day 1 versus context B on day 3 [treatment $F_{18,18} = 0.4932$; time $F_{2,18} = 12.84$; $P = 0.928$, not significant (n.s.)]. (**E**) Schematic of experiment to test effect of silencing LEC LRIPs on NOR. Mice were exposed to two objects in training trials 1 and 2, followed by a test trial in which one (now familiar or "old") object was replaced by a novel ("new") object. Before training, mice were infused with 0.5 μl of either 15 μM PSEM^{308} plus miniRuby (silenced group, + PSEM) or miniRuby alone (control). Both groups expressed PSAM in LEC. (**F**) Bar plots of time spent with familiar (old) versus novel (new) object in test trial. The PSEM-treated group explored the old object for 49.4 ± 3.6 s ($P < 0.005$ versus control) and the new object for 86.4 ± 7.5 s ($n = 6$; $P < 0.05$, new versus old object, paired t test). (**G**) The discrimination index, calculated as [(time spent exploring the new object) − (time spent exploring old object)]/(total exploration time), was significantly greater in control versus PSEM-treated mice ($P < 0.05$, paired t test).

hippocampus-dependent (*21*–*25*) (Fig. 2E). Mice were exposed to two objects during two 10-min training trials. After a 10-min delay, one of the now-familiar objects was substituted with a novel object, and the time spent exploring the novel versus familiar object was determined. The control group explored the old object for 25.6 ± 4.3 s and the new object for 66.3 ± 13.5 s ($n = 6$; $P < 0.05$, paired t test), which indicated object recognition memory. Similar to CFC, the LRIPs were not required for object memory storage as mice treated with PSEM during the training trials explored the novel object for a significantly longer time (86.4 ± 7.5 s) than they explored the familiar object (49.4 ± 3.6 s; $n = 6$; $P < 0.05$, paired t test) (Fig. 2F). However, the LRIPs were required for optimal memory storage, as the degree of memory performance, measured by the discrimination index for the two objects (Fig. 2G, see legend), was significantly greater for control (0.52 ± 0.06; $n = 6$) than for PSEM-treated mice (0.29 ± 0.06; $n = 6$; $P < 0.05$, paired t test). PSEM treatment also decreased the habituation that mice normally show to the objects during the

Corrected 21 January 2016; see full text.

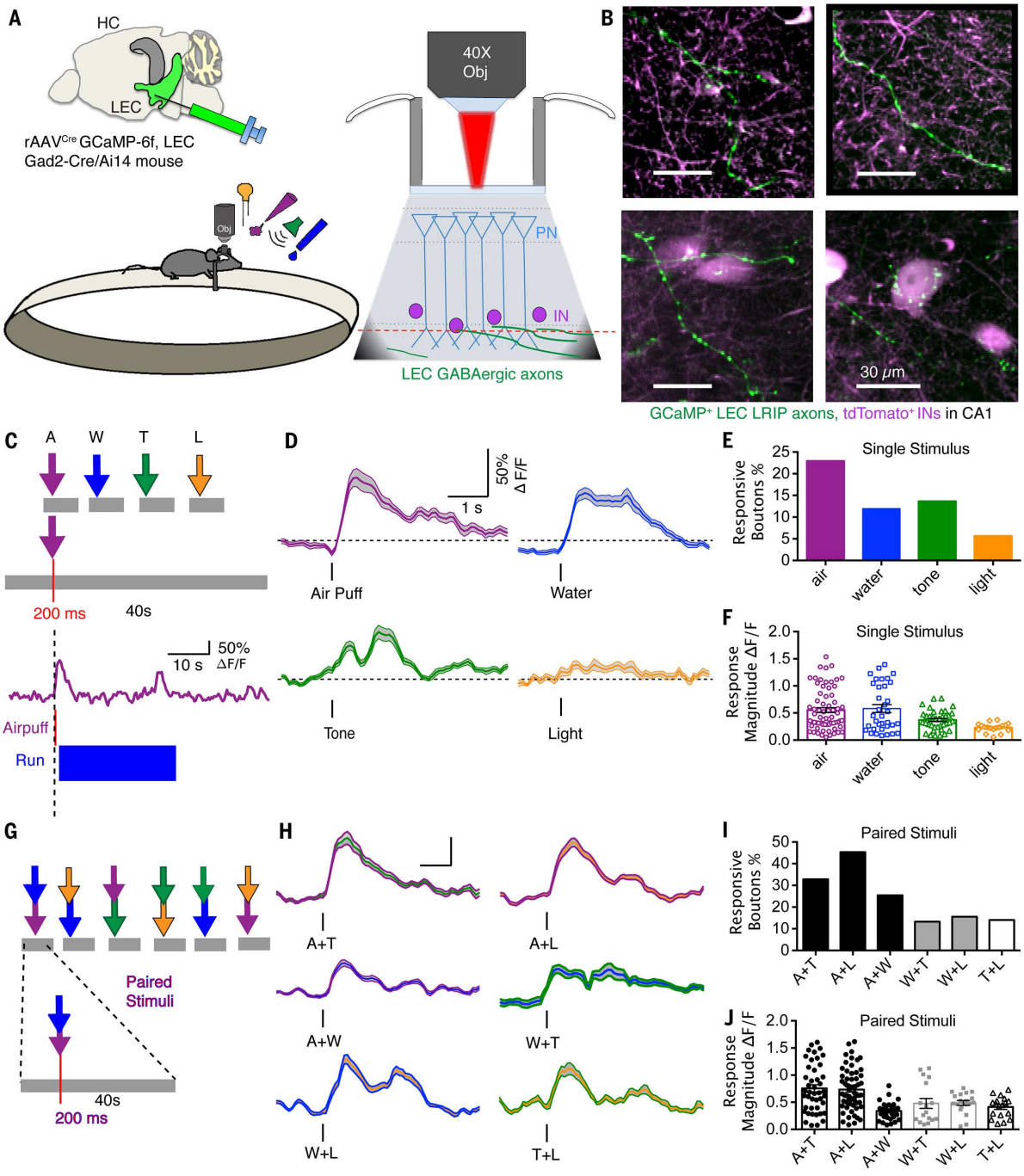

Fig. 3. Functional imaging of sensory coding in LEC LRIPs present in SLM of CA1. (**A**) Diagram of in vivo imaging experiment. GCaMP6f was expressed in dorsal LEC, by injecting Cre-dependent rAAV in *Gad2-Cre/Ai 14* mice that also expressed tdTomato in all GABAergic neurons. A 40× water immersion objective was used for two-photon imaging through a cranial window over CA1 in head-fixed awake mice during multimodal sensory and behavioral stimuli presentation. (**B**) Four examples of time-averaged images of GCaMP6f fluorescence in LEC LRIP axons in SLM (green) with tdTomato labeling CA1 interneurons (magenta). (**C**) Experimental design of single-stimulus protocol. Imaging was performed in blocks of four trials, each 40 s in duration. After a 10 ± 3 s baseline, one of four types of stimuli—aversive air puff (A), water drop (W), tone (T), or light (L)—was presented in random order for 200 ms, except the water drop was limited to 50 ms to prevent satiation. Each block was repeated to obtain at least five trials per stimulus. The animal's behavioral response (running and licking) was monitored. $\Delta F/F$ traces showing increased Ca^{2+} signal in a single bouton on an LRIP axon in response to air puff. (**D**) Mean (± SEM) $\Delta F/F$ Ca^{2+} signal (PSTH) from responsive ROIs to indicated stimuli. (**E**) Percentage of responsive boutons to the stimuli (air = 22.92%, water = 11.96%, tone = 13.64%, and light = 5.65%). (**F**) Scatter and mean (± SEM) plots of $\Delta F/F$ signals from individual responsive boutons (air = 0.55 ± 0.05, n = 68; water = 0.58 ± 0.07, n = 35; tone = 0.37 ± 0.03, n = 37; light = 0.23 ± 0.02, n = 18). (**G**) Experimental protocol: Imaging was performed as described above, but in response to pairs of stimuli, presented in blocks of 10 trials, each 40 s long. Stimuli were randomized and paired stimuli were interleaved with single stimulus presentations. (**H**) Mean (± SEM) $\Delta F/F$ Ca^{2+} signal (PSTH) from responsive ROIs to paired stimuli. (**I**) Percentage of responsive boutons for paired stimuli (A+T = 32.8%; A+L = 45.3%; A+W = 25.4%; W+T = 13.3%; W+L = 15.6%; T+L = 14.1%). (**J**) Scatter and mean (± SEM) plots of $\Delta F/F$ signals to paired stimuli from individual responsive boutons (A+T = 0.76 ± 0.07, n = 44; A+L = 0.74 ± 0.05, n = 58; A+W = 0.34 ± 0.03, n = 31; W+T = 0.48 ± 0.09, n = 17; W+L = 0.49 ± 0.04; T+L = 0.41 ± 0.045, n = 18).

second of the two training trials (fig. S7) ($P < 0.005$). Thus, although the LRIPs were not necessary for memory storage in two separate hippocampus-dependent nonspatial memory tasks, these inputs were important for enhancing the specificity of memory associations in performance of the two tasks.

LEC GABAergic inputs to CA1 are activated by sensory, motivational, and aversive stimuli in vivo

To explore how the LRIPs encode signals that might contribute to performance of nonspatial memory tasks, we used Ca^{2+} imaging to examine the responses of these inputs to a variety of sensory cues. We injected $rAAV^{Cre}$ in LEC of GAD2-Cre mice to express the genetically encoded Ca^{2+} indicator GCaMP6f (*26*) in GABAergic neurons. In vivo two-photon microscopy was then used to image Ca^{2+} signals in LRIP axons and axon terminals in the CA1 SLM region in response to a light stimulus, tone, aversive air puff, or water reward (Fig. 3, A to C) as described (*27*, *28*).

The sensory and behaviorally relevant stimuli elicited transient Ca^{2+} signals in LRIP axons and presynaptic boutons (Fig. 3, D to F), with the aversive air puff eliciting the largest increase in fluorescence intensity relative to the resting fluorescence intensity ($\Delta F/F = 0.55 \pm 0.05$) and greatest percentage of responsive boutons (22.9%). This result is of interest, as the aversive air puff is capable of serving as the unconditioned stimulus in a head-fixed CFC protocol (*28*). Water reward elicited a comparable Ca^{2+} signal in responsive boutons ($\Delta F/F = 0.58 \pm 0.07$) (movie S1), but only half as many boutons responded (11.9%) as compared with the response to the air puff.

As environmental contexts are composed of multisensory modalities, we also examined LRIP responses to pairs of stimuli (Fig. 3G). Paired stimuli tended to evoke larger Ca^{2+} responses in a greater fraction of boutons than did single stimuli. Pairing tone or light with air puff led to a 1.4-, 2.0-, and 3.2-fold greater Ca^{2+} response than when air puff, tone, or light were presented alone, respectively, with a 2- to 8-fold increase in the fraction of active boutons (Fig. 3, H to J). Whereas individual boutons usually responded to at most one or two of the four individual stimuli, collectively the LRIPs were able to represent the four sensory modalities examined (fig. S8D).

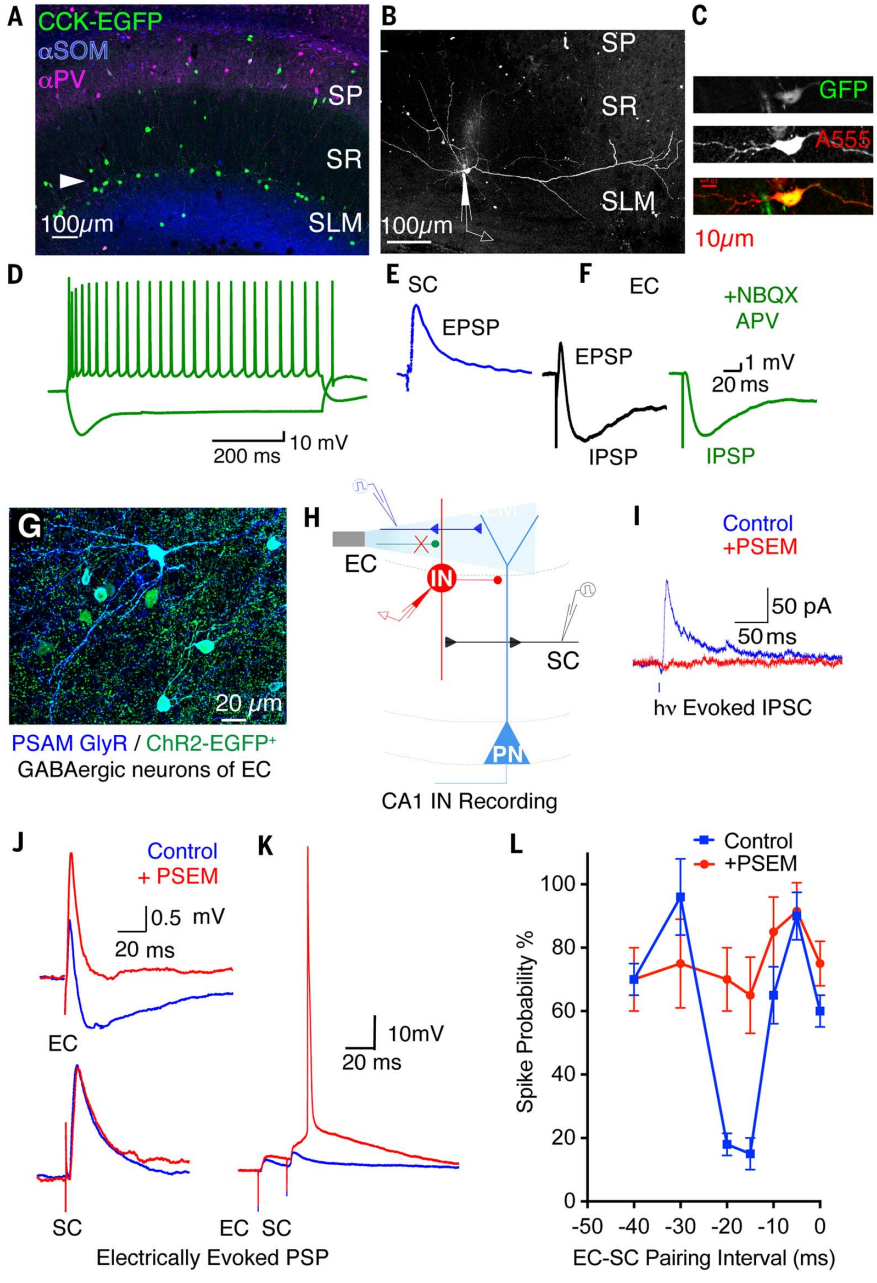

Fig. 4. CCK IN excitation and spike firing is suppressed 15 to 20 ms after LRIP activation. (**A**) Confocal projection image (left) showing CCK^+ (GFP, green), PV^+ (immunostained, magenta), and SOM^+ (immunostained, blue) IN soma in a hippocampal section from a *CCK-Cre/DLX-Flpe/RCE* dual-reporter mouse. Note abundant GFP^+ CCK IN soma at the SR-SLM border (arrowhead). (**B**) *Z*-axis projection image (right) of a GFP^+ CCK IN at SR-SLM border filled with neurobiotin-Alexa 555 (white). (**C**) Zoomed in image of IN in (B), showing GFP (top) and Alexa 555-neurobiotin (middle) colabeling (bottom, yellow). Scale bar, 10 μm. (**D** to **F**) Whole-cell voltage recordings from IN in (B) and (C). (D) Spike firing and voltage sag in response to 700-ms, 200 pA depolarizing and hyperpolarizing current steps, respectively. (E) Depolarizing PSP evoked by SC stimulation. (F) Mixed depolarizing and hyperpolarizing PSP evoked by EC stimulation (black). Bath application of NBQX (10 μM) and D-APV (100 μM) blocked the depolarization but not the hyperpolarization (green trace). (**G**) A 63× projection image of PSAM (α-bungarotoxin Alexa 647, blue) and ChR2-EGFP (green) showing coexpression in ~75% of EC INs in horizontal brain section from a *Gad2-Cre* mouse injected in LEC and MEC with $rAAV^{Cre}$. (**H**) Experimental scheme showing whole-cell recording from a CA1 SR-SLM IN with photostimulation of LRIPs or electrical activation of EC inputs. (**I**) Voltage-clamped IPSCs (at +10 mV) from CCK^+ IN (verified by post hoc staining) evoked by photostimulation of LRIPs in the absence (blue trace) or presence (red trace) of PSEM (3 μM). (**J**) Voltage responses in CA1 IN evoked by electrical stimulation of EC (top) or SC (bottom) inputs in the absence (control, blue trace) or presence (red trace) of PSEM. (**K**) Voltage responses of CA1 SR-SLM IN to paired electrical stimulation of EC and SC inputs (20-ms delay) in the absence (blue trace) or presence (red trace) of PSEM. (**L**) Mean probability of SR-SLM IN spike firing (percent of stimuli eliciting a spike ±SEM) in response to paired EC-SC stimulation as a function of pairing interval in the absence and presence of PSEM (spike probability with −20-ms EC-SC pairing: control = 18 ± 4%; PSEM = 70 ± 10%; $P < 0.005$, $n = 7$).

Corrected 21 January 2016; see full text.

Moreover, the probability that a single bouton responded to three distinct pairs of stimuli was higher than predicted from a random, independent distribution of boutons based on the measured response to individual pairs of stimuli. Thus, a subpopulation of LRIPs may be specifically tuned to encode multimodal sensory cues, similar to what constitutes a behavioral context.

Spontaneous motor behaviors, such as spontaneous running and licking, also elicited Ca^{2+} responses in the LRIPs (fig. S8E). Although the aversive air puff typically elicited a running response, the air puff recruited a greater fraction of boutons and evoked a larger Ca^{2+} signal compared with that seen with spontaneous running. This indicates a specific sensory contribution to the air-puff response. Furthermore, LRIP boutons that made apparent contacts on dendrites had larger Ca^{2+} responses than did boutons that targeted SR-SLM interneuron somata (fig. S8, F and G).

We wondered why different boutons showed such diverse responses to different stimuli. One clue came from the finding that boutons along a single axon responded more uniformly to a set of sensory cues than did neighboring boutons from different axonal fibers (fig. S8, H and I). This indicated that the variability in bouton response was likely not caused by random trial-to-trial variability but rather resulted from the specific tuning of individual LRIP axons to distinct combinations of sensory and behavioral cues. This finding is consistent with the idea that these inputs are important for regulating nonspatial contextual and object memory.

LRIPs from LEC transiently inhibit spike output of local CA1 dendrite-targeting feedforward inhibitory neurons

How do the long-range GABAergic projections influence information flow through the cortico-hippocampal circuit to regulate memory storage? We began to investigate this question by performing whole-cell recordings from cholecystokinin-positive (CCK^+) SR-SLM interneurons, which represent a large fraction of the SR-SLM border INs targeted by the LRIPs (fig. S9). Moreover, the CCK^+ INs receive strong excitatory drive from the SCs and send strong inhibitory output to CA1 pyramidal neuron dendrites (*11*, *29*, *30*).

To determine how the CCK^+ INs integrate their cortical and hippocampal inputs, we electrically stimulated the SC axons (using an electrode in SR) or a mixed population of excitatory and inhibitory EC axons (using an electrode in SLM). We then recorded the synaptic responses in genetically defined CCK^+ SR-SLM INs tagged with GFP (*11*, *16*) (Fig. 4, A to C). These neurons displayed a large voltage sag in response to hyperpolarization and an intermediate firing pattern, characteristic of CCK^+ INs (*29*, *31*–*33*) (Fig. 4D).

SC stimulation elicited a strongly depolarizing PSP in the CCK^+ INs, with a peak amplitude of 9.83 ± 0.17 mV at 50% maximal stimulation strength (Fig. 4E). In contrast, EC stimulation evoked a mixed EPSP-IPSP (inhibitory postsynaptic potential peak depolarization of 0.79 ± 0.34 mV) that was dominated by a large hyperpolarization, which reached its peak negative value (–5.59 ± 0.17 mV, n = 7) ~20 ms after the stimulus (Fig. 4F). As we show below, the time course of the hyperpolarization imposes a precise timing dependence for disinhibition, which regulates the timing of the induction of ITDP and the generation of dendritic spikes in response to paired stimulation of the EC and SC inputs. The EC-evoked IPSP was unaffected by blockers of glutamatergic transmission NBQX 10 μM and 2-amino-5-phosphonovaleric acid (APV) 100 μM, which demonstrated that it resulted from direct activation of GABAergic axons rather than disynaptic FFI (Fig. 4F).

To determine whether the electrically evoked IPSP in CA1 INs was caused by GABA release from the EC LRIPs, we silenced these projections using the PSAM-PSEM approach (Fig. 4, G and H). Two independent $rAAV^{Cre}$ vectors expressing ChR2 and PSAM were injected into LEC and MEC of Gad2-Cre mice (Fig. 4G). The light-evoked IPSC recorded from SR-SLM INs was fully blocked by local bath application of 3 to 5 μM $PSEM^{308}$ (IPSC = 0.013 ± 0.04 pA, n = 11), which verified

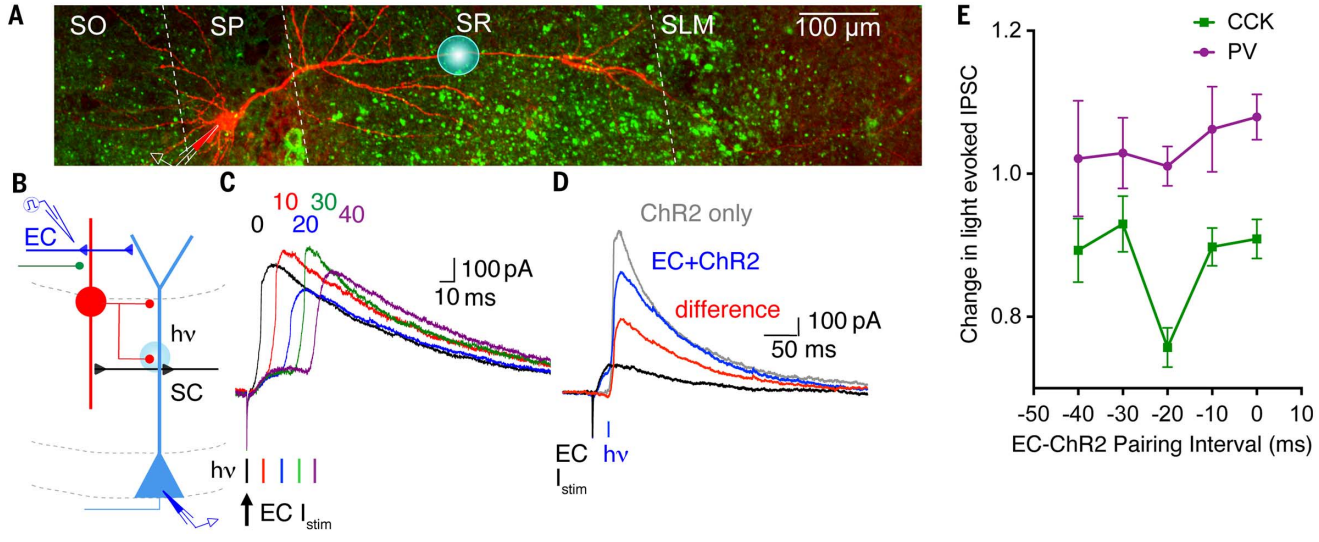

Fig. 5. LRIPs suppress SC-evoked FFI from CCK^+ SR-SLM INs. (**A**) Confocal projection image of a CA1 PN filled with Alexa 594 (red) in a slice where CCK^+ INs expressed ChR2-EGFP (green). Blue circle represents the perimeter of 470-nm light stimulus. (**B**) Experimental scheme depicting somatic recording from a CA1 PN (red); electrical stimulation of EC inputs in SLM was paired at variable delays with photostimulation of CCK^+ INs. (**C**) IPSCs evoked by photostimulation of CCK^+ INs (*hv*) recorded from soma of a voltage-clamped CA1 PN (+10 mv) during paired electrical stimulation of EC inputs (arrow) at 0, 10-, 20-, 30-, and 40-ms delays. (**D**) IPSCs in CA1 PNs evoked by electrical stimulation of EC inputs and photostimulation of CCK^+ INs. Gray trace (ChR2 only), CA1 PN IPSC evoked by photostimulation of CCK^+ IN. Black trace (EC), CA1 PN IPSC evoked by electrical stimulation of EC input. Blue trace (EC+ChR2), net IPSC evoked by pairing EC electrical stimulation with photostimulation of CCK^+ IN (20-ms delay). Red trace (difference), inferred CCK^+ IN IPSC evoked when EC electrical stimulation preceded photostimulation of CCK^+ IN by 20 ms. Trace obtained by subtracting EC-evoked IPSC (black trace) from IPSC evoked during paired stimulation (blue trace). (**E**) Effect of pairing interval on EC-dependent suppression of IPSC evoked by photostimulation of CCK^+ INs or PV^+ INs. Mean (±SEM) amplitude of photostimulation-evoked IPSC during pairing with EC stimulation [measured as in (D)] normalized by photostimulated IPSC amplitude in the absence of EC stimulation, plotted versus pairing interval. ChR2-EGFP expressed in either PV^+ INs (magenta, 1.01 ± 0.03-fold change at –20-ms pairing interval, P = 0.3319, paired two-tailed t test, n = 5) or CCK^+ INs (green, 0.76 ± 0.03-fold decrease in IPSC at –20-ms pairing interval, $P < 0.001$ paired two-tailed t test, n = 9).

the efficacy of this method (Fig. 4I). Silencing the LRIPs nearly abolished the hyperpolarizing component of the mixed PSP evoked by electrical stimulation (peak negative value reduced to –0.29 ± 0.21 mV, n = 7), whereas it increased the peak depolarization during the PSP (to 4.79 ± 0.79 mV), which demonstrated the importance of this projection. PSEM caused no change in the PSP evoked by electrical stimulation of the SC axons in SR (Fig. 4J), which indicated the specificity of the approach.

Does LRIP activation affect action potential output of the SR-SLM INs in response to paired stimulation of their EC and SC inputs? Electrical stimulation of the EC pathway alone failed to trigger spike firing (Fig. 4K), consistent with the weak depolarizing phase of the mixed EPSP-IPSP response (Fig. 4F). In contrast, moderately strong stimulation of the SC pathway alone (50 μA stimulus current injection) elicited a large depolarizing PSP that triggered a spike in SR-SLM INs with >50% probability (Fig. 4L). However, when the SC stimulus was preceded by a stimulus to the EC inputs that occurred 15 to 20 ms before stimulation of the SC inputs, the ability of the SC inputs to trigger action potentials in the SR-SLM INs was suppressed (Fig. 4, K and L). The timing dependence of spike suppression (Fig. 4L) coincided with the maximal hyperpolarization of the SR-SLM INs in response to EC stimulation, which suggested that the suppression of spike firing was mediated by the activation of the LRIP inputs. Consistent with this idea, silencing the LRIPs with PSAM-PSEM prevented the suppression of spike firing upon electrical stimulation of the EC inputs (Fig. 4, K and L).

LRIPs provide a temporally precise gate of hippocampal input to CA1 pyramidal neurons

What are the consequences of the LRIP-mediated suppression of SR-SLM IN firing for the activity of CA1 pyramidal neurons? To examine this question, we virally expressed ChR2 in CCK$^+$ INs in the CA1 SR/SLM region and measured the light-evoked IPSC in CA1 pyramidal neurons voltage-clamped at +10 mV (Fig. 5, A and B). Photostimulation of the CCK$^+$ INs with a light pulse focused in SR produced a robust IPSC in the

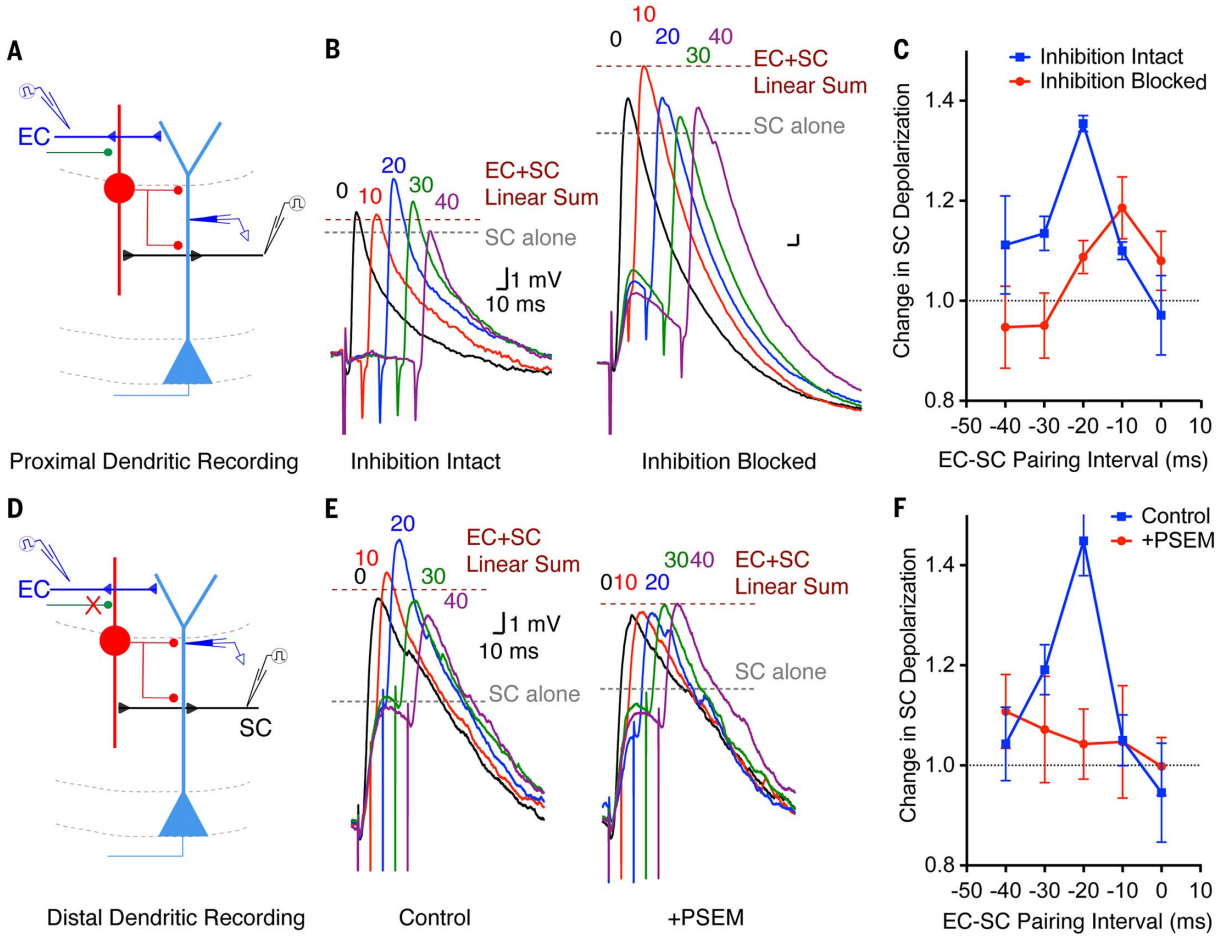

Fig. 6. LRIPs enhance CA1 pyramidal neuron dendritic depolarization in response to SC stimulation through disinhibition. (**A**) Experimental scheme for assessing the synaptic response in CA1 PN dendrites to paired EC-SC electrical stimulation. Horizontal lines show approximate locations of EC and SC stimulation electrodes and dendritic recording pipette. (**B**) Dendritic voltage responses to paired EC-SC electrical stimulation at indicated delays (SC after EC), in the absence (left) or presence (right) of GABAR antagonists SR 95531 (2 μM) and CGP 55845 (1 μM). Gray dashed line, amplitude of PSP evoked by SC stimulation alone. Red dashed line, predicted linear sum of PSPs evoked by EC and SC paired stimulation. (**C**) Summary plot (mean ± SEM) of paired EC-SC peak PSP normalized by PSP evoked by SC stimulation alone recorded in CA1 PN proximal dendrites. PSPs measured in the absence (blue squares) and presence (red circles) of GABAR blockers (EC-SC –20-ms pairing: with inhibition intact, fold change = 1.35 ± 0.02; with inhibition blocked, fold change = 1.08 ± 0.03; P = 0.001, two-way ANOVA with Sidak multiple comparisons test, n = 5). (**D**) Experimental scheme to determine how silencing LRIPs (denoted by X) affects PSP in CA1 PN distal dendrites during paired EC-SC stimulation. PSAM expressed in LEC GABAergic neurons in *GAD2-Cre* mouse with AAV^{Cre}. (**E**) CA1 PN distal dendrite PSPs evoked by paired stimulation of EC-SC inputs at indicated intervals, first in the absence (left) and then the presence (right) of PSEM. (**F**) Mean (± SEM) PSP amplitude recorded in CA1 PN distal dendrites evoked by paired EC-SC stimulation normalized by PSP evoked by SC stimulation alone, in the absence (blue squares) and presence (red circles) of PSEM. PSEM significantly reduced the effect of paired EC-SC stimulation at –20-ms delay to increase PSP size (control, 1.45 ± 0.07-fold increase; PSEM, 1.04 ± 0.07-fold increase; P < 0.001, two-way ANOVA with Sidak multiple comparisons test, n = 8).

Corrected 21 January 2016; see full text.

CA1 pyramidal neuron soma (~250 μm from the light spot). Electrical stimulation of the EC inputs 20 ms before photostimulation significantly suppressed the light-evoked IPSC (to 75.6 ± 2.7% of the unpaired light-evoked IPSC, n = 9; P < 0.0001, two-way ANOVA) (Fig. 5, C to E), with little change at other pairing intervals. Electrical stimulation did not alter the light-evoked IPSC when ChR2-EYFP was expressed in PV$^+$ INs, regardless of pairing interval, which indicated the specificity of the effect. As ChR2 photostimulation provides an unusually strong excitatory drive compared with an action potential, the LRIPs are likely to produce an even greater suppression of the CCK$^+$ IN–mediated IPSP evoked by excitatory synaptic input.

Does the suppression of CCK$^+$ IN firing by the LRIPs influence the ability of the EC or SC inputs to excite CA1 pyramidal neurons? As the SR-SLM INs are known to target CA1 pyramidal neuron apical dendrites, we addressed this question using whole-cell recordings from CA1 pyramidal neuron dendrites 150–300 μm from the soma in SR during single or paired stimulation of the EC and SC inputs (Fig. 6).

Stimulation of the SC input alone evoked a large depolarizing PSP in the proximal dendrite ~150 μm from the soma (4.48 ± 0.57 mV, n = 5) (fig. S10). Stimulation of the EC input alone evoked only a very small dendritic depolarization (1.00 ± 0.24 mV) (fig. S10). However, when we stimulated the EC input 20 ms before the SC input, we observed a supralinear boosting of dendritic depolarization (Fig. 6, B and C), which resulted in a net PSP that was 1.35 ± 0.02 times the PSP evoked by stimulation of the SC pathway alone. This boost was significantly greater than the predicted linear sum of 1.13 ± 0.024-fold for the SC response alone (P < 0.05, t test; n = 5). Paired EC-SC stimulation at the –20-ms interval was associated with an even greater 2.2-fold increase in the postsynaptic Ca^{2+} transient evoked by SC stimulation in CA1 pyramidal neuron dendritic spines in SR, relative to the Ca^{2+} transient elicited by SC input alone (fig. S10) (P < 0.001, t test, n = 5).

It was striking that the supralinear boosting was sharply tuned to the –20-ms pairing interval. Paired activation of EC and SC inputs at other intervals resulted in linear or sublinear summation (Fig. 6, B and C). Moreover, pairing at the –10-ms interval produced a significantly lower boosting in spine Ca^{2+} compared with the –20-ms interval (1.3-fold, P < 0.0001, t test, n = 5).

The timing dependence of the supralinear boosting of the CA1 pyramidal neuron PSP suggested to us that it might result from a disinhibitory action of the LRIPs to suppress SC-evoked FFI through the SR-SLM INs (Fig. 6D). We therefore compared the effect of paired EC-SC stimulation before and after application of GABA receptor channel antagonists (Fig. 6, B and C). Blockade of inhibition greatly increased the peak depolarization during the PSP evoked by stimulation of the EC and/or SC inputs, reflecting the removal of FFI (Fig. 6B and fig. S10, B and C). Of note, paired EC-SC stimulation produced only a linear or sublinear summation at all pairing intervals in the presence of the antagonists, consistent with the view that supralinear summation was caused by disinhibition. For example, pairing at a –10-ms interval resulted in a net PSP 1.19 ± 0.06 times that of the SC PSP alone and not significantly different from the linear sum of the EC+SC PSPs when stimulated independently (P = 0.238). In addition, the peak of the paired response was shifted to the –10-ms pairing interval, which corresponds to the expected peak of temporal summation of the individual EC and SC EPSPs.

Next, we tested directly whether the LRIPs were responsible for the supralinear boosting by recording PSPs in distal CA1 pyramidal neuron dendrites (300 μm from the soma) in response to paired EC-SC stimulation, before and after silencing the LRIPs (Fig. 6, D to F). We found that application of PSEM^{308} (3 μM) to slices in which the LRIPs expressed PSAM fully prevented the supralinear boosting (Fig. 6, E and F). Thus, we propose that the EC LRIPs potentiate the ability of the SC inputs to excite CA1 pyramidal neuron dendrites by suppressing SC-evoked feedforward inhibition mediated by the SR-SLM interneurons.

Disinhibition through LEC LRIPs enables input timing–dependent plasticity and dendritic spike firing

Given the behavioral role of the LRIPs in memory storage, we asked whether these inputs may also contribute to more robust, longer-lasting forms of SC input gating than the transient boosting of dendritic depolarization and spine Ca^{2+} levels seen above. Paired EC-SC stimulation at 1 Hz for 90 s induces a long-lasting form of heterosynaptic plasticity, termed input timing–dependent plasticity (ITDP) which strongly enhances SC-evoked excitation of the CA1 pyramidal neuron through combined long-term potentiation of the SC EPSP and long-term depression of inhibition mediated by somatic-targeting CCK$^+$ basket cells (which are distinct from the CCK$^+$ SR/SLM INs) (*10*, *11*). As the induction of ITDP is finely tuned to the same –20-ms pairing interval optimal for LRIP-mediated disinhibition, we hypothesized that the LRIPs from EC may be required for this plasticity. In support of this view, we found that silencing of PSAM-expressing LRIPs, either from LEC alone or from both LEC and MEC, with PSEM^{308} fully blocked the induction of ITDP (Fig. 7, A and B).

The above results suggest that the induction of ITDP is normally suppressed by FFI evoked by SC stimulation and, thus, requires LRIP activation to suppress this inhibition. This model would also explain how the induction of ITDP is finely tuned to the –20-ms pairing interval. This scenario predicts that robust ITDP may be induced over a broader range of intervals when EC-SC paired stimulation is given in the presence of GABAR antagonists, which would eliminate FFI at all pairing intervals. Consistent with this model, we found that the presence of GABAR blockers

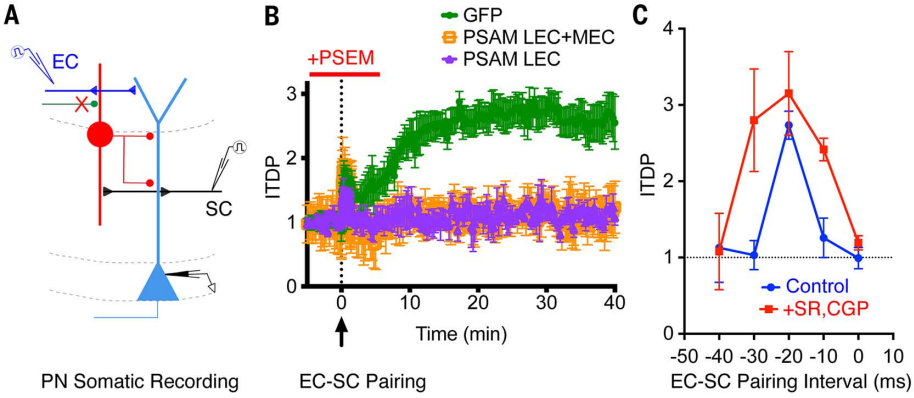

Fig. 7. LEC LRIPs enable induction of ITDP in CA1 PNs. (**A**) Experimental scheme to assess role of LRIPs in ITDP. PSAM or GFP was expressed in GABAergic neurons in LEC alone or in both LEC and MEC. ITDP was induced by pairing EC-SC stimulation at 1 Hz for 90 s with a –20-ms delay. (**B**) Pairing protocol induces a 2.65 ± 0.23-fold increase in the SC-evoked depolarization in the CA1 PN soma (ITDP relative to baseline PSP) when PSEM is applied to slices expressing GFP in LEC GABAergic neurons (green, n = 5, P < 0.0001, two-tailed t test, before versus after ITDP pairing). ITDP is absent when the pairing protocol is applied with PSEM present in slices expressing PSAM in GABAergic neurons in LEC alone (purple triangles, 1.09 ± 0.12-fold potentiation, n =4, P = 0.114, two-tailed t test before versus after ITDP pairing; P < 0.0001, two-tailed t test for ITDP with GFP versus PSAM in LEC). ITDP is also absent in the presence of PSEM when PSAM was expressed in both LEC and MEC (orange squares, 1.10 ± 0.31-fold potentiation, n = 4, P = 0.189, two-tailed t test pre versus post ITDP pairing; P < 0.0001, two-tailed t test for ITDP with GFP versus PSAM in LEC+MEC). Peak PSP value normalized to value 5 min before ITDP induction. Mean fold potentiation obtained by averaging normalized PSP values during the 25- to 30-min period after ITDP induction. (**C**) ITDP tuning curve showing potentiation (mean ± SEM) as a function of EC-SC pairing interval. Blue circles, with inhibition intact (–10-ms interval, 1.25 ± 0.26-fold change, n = 4; –20-ms interval, 2.74 ± 0.18-fold change, n = 5; –30-ms interval, 1.03 ± 0.19-fold change, n = 4). Red squares, ITDP with GABAR antagonists applied only during induction protocol (–10 ms, 2.41 ± 0.15-fold change, n = 5; –20 ms, 3.15 ± 0.55-fold change, n = 7; –30 ms, 2.8 ± 0.67-fold change, n = 4). Inhibition blocked versus intact, no significant difference, P = 0.105 two way ANOVA –20, –10, and –30 ms comparison.

during the ITDP induction protocol alone enabled the induction of robust ITDP over a broader range of pairing intervals, from –10 to –30 ms (Fig. 7I). This ITDP tuning curve now matched the expected time course of temporal summation of the EC and SC EPSPs (*10*).

How could the relatively modest boosting by the LRIPs of the EC-SC synaptic depolarization lead to such a robust form of plasticity? Many forms of long-term synaptic plasticity that do not depend on somatic action potentials [such as ITDP (*10*, *11*)] require the firing of dendritic spikes, which can enhance Ca^{2+} influx into the postsynaptic cell (*34*, *35*). Thus, we next examined whether more prolonged EC-SC pairing, as used to induce ITDP, promoted dendritic spiking, using whole-cell recordings from distal CA1 pyramidal neuron dendrites (≥300 μm from the soma) (Fig. 8A).

Although single paired–EC-SC stimulation failed to elicit a dendritic spike, large regenerative spikes began to appear when we delivered 10 or more paired EC-SC stimuli at 1 Hz using a –20-ms interval (Fig. 8B). Event amplitude frequency histograms (Fig. 8C) showed three peaks, corresponding to subthreshold PSPs (~20 mV amplitude); small, brief action potentials (~40 mV) resembling dendritic Na^+ spikes (*34*, *36*); and longer, larger events (~60 mV) resembling dendritic Ca^{2+} spikes (*34*, *36*, *37*). Both types of spikes were preferentially generated at the –20-ms pairing interval compared with a –10-ms pairing interval. Both types of spikes also required LRIP input as spike probability greatly decreased when the LEC LRIPs were silenced with PSAM-PSEM (Fig. 8, D to F).

Experiments using two-photon Ca^{2+} imaging in CA1 pyramidal neurons supported the view that the dendritic spikes may contribute to the induction of ITDP. Repetitive stimulation of EC-SC inputs at 1 Hz using a –20-ms pairing interval led to long-lasting Ca^{2+} signals in the apical dendrites that propagated to the soma (fig. S10, F and G). These dendritic signals provide a likely source for the intracellular Ca^{2+} required for the induction of ITDP (*10*, *11*). Pairing-induced dendritic spikes gated by the LRIPs may thus provide a powerful nonlinear mechanism for the long-term enhancement of SC-mediated excitation in response to temporally precise, coordinated cortico-hippocampal dendritic activity.

Discussion

The importance of excitatory projections from LEC and MEC to hippocampus for memory storage and spatial encoding is well established (*38*). MEC also sends LRIPs to hippocampus that form synapses on CA1 SR-SLM GABAergic interneurons (*4*), although the in vivo function of these inputs was not determined. Here, we report that LEC sends LRIPs to CA1 that exert an even stronger inhibitory drive on CA1 SR-SLM INs than the LRIPs from MEC. We also found that LRIPs from LEC convey multimodal sensory information that helps fine-tune the specificity of hippocampus-dependent contextual memory storage and enhances the ability to distinguish novel from familiar objects. Finally, the LRIPs provide a temporally precise disinhibitory gating mechanism for enhancing information flow within the hippocampal circuit at both short and long time scales.

Within the context of the cortico-hippocampal circuit, the LRIPs transiently suppress dendritic FFI to enhance excitatory signals from the trisynaptic path that arrive at CA1 pyramidal neurons precisely 20 ms after LRIP activation. The effect of this disinhibitory gating has ramifications across widely different time scales. Activation of the LRIPs with a single pairing of EC-SC stimulation at a –20-ms interval causes a transient supralinear boost in local dendritic depolarization and proximal spine Ca^2. Repetitive paired stimulation of EC and SC inputs at the same interval leads to further amplification of synaptic input by promoting the firing of dendritic spikes (*8*, *9*) and the induction of ITDP, a robust Ca^{2+}-dependent form of long-term heterosynaptic plasticity (*10*, *11*). Given that dendritic spikes are normally suppressed by strong FFI (*9*), the ability of the LRIPs to enhance dendritic spiking during a precise temporal window may contribute to the dendritic spike firing in vivo observed during behaviorally relevant cooperative activity (*39*). The LRIP-dependent

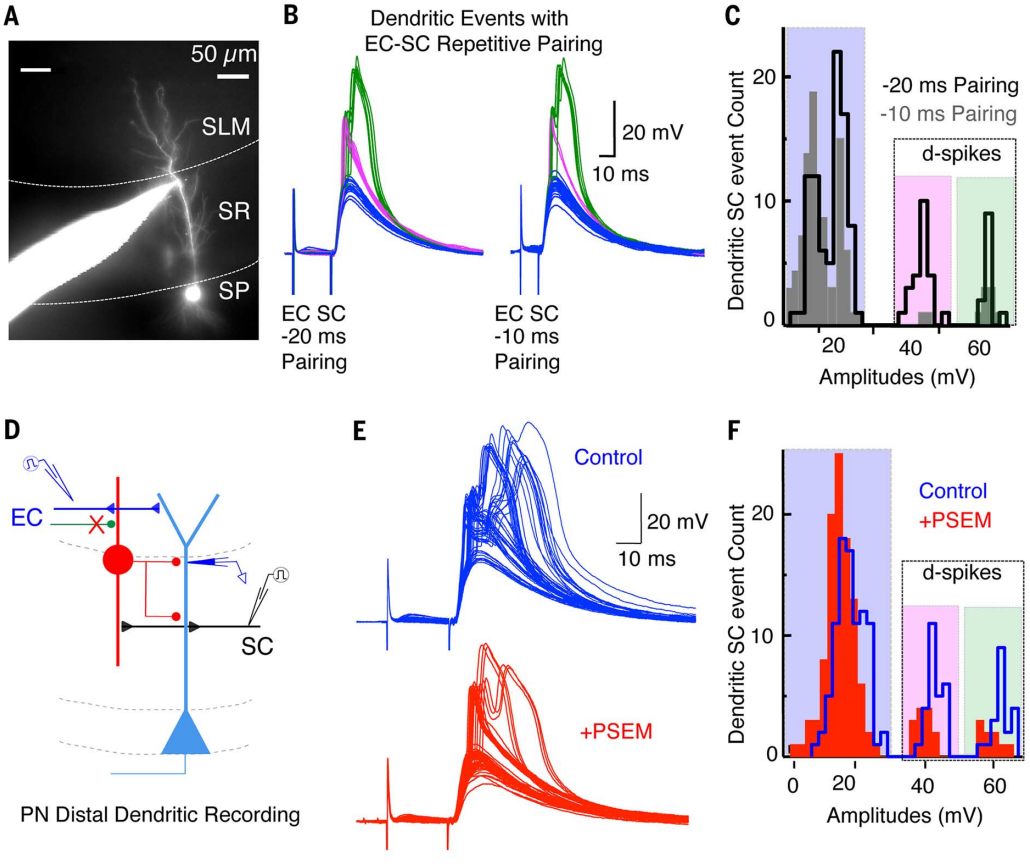

Fig. 8. EC-SC pairing at –20-ms interval induces dendritic spikes. (**A**) Image showing CA1 PN filled with Alexa 594 during a distal dendritic recording. (**B**) Dendritic PSPs (blue), brief spikes (magenta), and long spikes (green) evoked by 10- to 30-s repetitive pairing of EC-SC inputs at 1 Hz with –20- or –10-ms pairing intervals. During the first 5 to 10 paired stimuli, only subthreshold PSPs (blue) were observed. Subthreshold PSPs, brief spikes, and long spikes were then observed interspersed with subsequent paired stimuli. (**C**) Histograms of the peak dendritic voltage response evoked by a train of 30 paired EC-SC stimuli at 1 Hz, by using a –20-ms (black open bars) or –10-ms (gray filled bars) pairing interval ($P < 0.005$, t test within cell comparisons for –20 ms vs –10 ms; $n = 3$). Responses were classified on the basis of amplitude and duration as subthreshold PSPs (blue) or dendritic spikes (magenta, brief spikes; green, long spikes. (**D**) Experimental scheme to assess the role of LRIPs in dendritic spike firing. PSAM was virally expressed in LEC of Gad2-Cre mice. (**E** and **F**) Distal dendritic responses (E) and event amplitude histograms (F) to paired EC-SC stimulation at 1 Hz by using a –20-ms delay interval in the absence (blue) and then presence (red) of PSEM ($P < 0.0001$, t test within cell comparisons, control vs. +PSEM; $n = 3$).

Corrected 21 January 2016; see full text.

dendritic spikes are likely to participate in the induction of ITDP and the fine-tuning of learning and memory; this likelihood is based on the role of such spikes in both other forms of Ca^{2+}-dependent synaptic plasticity (*34*, *35*, *40*) and nonlinear gain modulation during associative learning (*35*) and sensory tuning (*41*).

Our findings, together with previous results (*28*, *42*–*45*), further demonstrate how distinct populations of local interneurons play well-defined roles in hippocampus-dependent behaviors and circuit function. We found that CCK^+ INs located near the SR-SLM border exert strong FFI onto CA1 pyramidal neuron dendrites; LRIP-mediated transient suppression of these INs enables temporally precise supralinear dendritic excitation. The GABAR kinetics, CA1 pyramidal neuron membrane time constant (*29*, *46*), and in vivo firing patterns (*47*) of the CCK^+ INs are all likely to participate in ensuring that the kinetics of the LRIP-mediated IPSP are appropriately tuned to implement the 20-ms gating of information flow from the SC inputs to CA1 pyramidal neurons. Of note, mice have been found to display an overgeneralized contextual learning phenotype when signaling in CA1 CCK^+ INs is perturbed (*48*), similar to our behavioral findings when the LRIPs that target these INs are silenced.

The role of the CCK^+ SR-SLM border INs in implementing the ITDP timing rule contrasts with the role in ITDP of a separate subclass of CCK^+ INs, the perisomatic-targeting basket cells located in and around the CA1 pyramidal neuron cell body layer (*11*). Previously, we found that the expression of ITDP results from the combined effects of long-term potentiation of the SC excitatory synapses on CA1 pyramidal neurons and the long-term depression of FFI from a population of perisomatic-targeting CCK^+ basket cell INs onto the same CA1 pyramidal cells (*11*). Thus, anatomically distinct subpopulations of the same genetically defined class of CCK^+ INs are specifically involved in the induction versus the expression of ITDP. Yet another class of CA1 INs, the somatostatin-positive (SOM^+) dendrite targeting INs, has been found to be required for CFC (*28*). These INs serve to suppress EC input to CA1 pyramidal neuron dendrites during aversive stimuli, thereby ensuring that the unconditioned stimulus is not encoded as part of the contextual representation. Thus, distinct populations of GABAergic INs participate in distinct microcircuits to regulate separate phases of memory encoding.

What is the significance of the precise 20-ms temporal window for LRIP-dependent disinhibitory gating? One interesting possibility is suggested by the fact that this interval is matched to the dynamics of the delay-line architecture of the cortico-hippocampal circuit, where signals propagating through the trisynaptic path arrive at CA1 pyramidal neurons about 15 to 20 ms after the arrival of signals through the direct path (*49*). Thus, the temporal dynamics of LRIP-mediated disinhibition will enhance the propagation to a given CA1 pyramidal neuron of those signals arriving through the trisynaptic path that were initiated by activity in EC LII stellate cells (which project to dentate gyrus) simultaneously with activity in the subset of EC LII (*3*) and LIII pyramidal neurons (*6*) that directly project to the same CA1 pyramidal neuron. This timing rule for disinhibitory gating may therefore serve as a filter to assess the salience of processed associations arriving from CA3 inputs on the basis of their temporal relation to the direct multimodal sensory inputs arriving from EC.

Because our studies of the effects of LRIP activation on CA1 pyramidal neuron function were carried out in ex vivo hippocampal slices, a key question is whether the 20-ms timing interval between cortical and SC input that is required for the boosting of SC excitation is implemented by in vivo patterns of cortico-hippocampal activity. Studies of the temporal relation of oscillatory activity in entorhinal cortex and hippocampus in vivo suggest that the disinhibitory gating mechanism may indeed be engaged during spatial behavior (*50*, *51*) and associational learning (*52*). For example, during running and memory tasks, fast gamma oscillations (100 Hz) arising from EC LIII are observed in SLM of CA1 and precede the slow gamma oscillations (50 Hz) in SR of CA1, which are thought to reflect CA3 pyramidal neuron input (*50*). Notably, EC LIII–CA1 gamma activity and CA3-CA1 gamma activity display a 90° phase offset during theta frequency oscillations (8 to 9 Hz) (*50*) that is consistent with a ~20- to 25-ms time delay.

Learning is a critical adaptive behavior, and the precision of memory storage normally enables an animal to discriminate between harmful (salient) versus safe (neutral) environments. Failure to do so can lead to overgeneralization of fear memories, a characteristic feature of posttraumatic stress and other anxiety disorders. How might the effect of the LRIPs to enhance cortico-hippocampal information flow contribute to their behavioral role to enhance learning specificity? The increased freezing in the conditioned and novel contexts upon silencing the LRIPs indicates that the disinhibitory circuit, and by implication ITDP, is not required for generalized fear learning, which may be implemented by other intrahippocampal circuits (*28*, *53*) or other forms of plasticity, such as SC Hebbian LTP. Similarly, the LRIPs are not needed for basic object recognition memory. Rather, we suggest that the LRIPs may enhance contextual and object memory storage and may improve memory specificity by creating a sparse, high-contrast ensemble of potentiated SC synapses whose dynamics conform to the temporal window of paired EC-SC associative inputs that enables the induction of ITDP.

Materials and Methods

All experiments were conducted in accordance with the National Institutes of Health guidelines and with the approval of the Columbia University and New York State Psychiatry Institute (NYSPI) Institutional Animal Care and Use Committee.

Mice

Gad2-IRES-Cre (*16*), PV-IRES-Cre (*54*), and Ai14-tdTomato (*55*) mouse lines were obtained from the Jackson Laboratory (JAX); IRES refers to internal ribosomal entry site. The CCK IN-specific enhanced green fluorescent protein (EGFP)–labeled line was generated as described in references (*11*, *16*). Briefly, CCK-IRES-Cre driver mice (generous gift of Z. J. Huang, Cold Spring Harbor Laboratory) (*11*, *16*) were crossed with the Dlx5/6-Flpe driver mice [generous gift from G. Fishell, New York University (*56*)] and a Cre- and Flp-dependent EGFP reporter strain, R26NZG [JAX (*57*)].

Viruses

For anatomy and slice electrophysiology experiments in Fig. 1, we used the following: (i) rAAV2/1 EF1α-DIO-ChR2-EYFP (K. Deisseroth, Stanford University), (ii) AAV2/9 CAG-Flex-EGFP, and (iii) rAAV2/9 CAG-Flex-tdTomato [all prepared by University of Pennsylvania (UPenn) Vector Core]. Behavioral experiments in Fig. 2 utilized: (i) for the PSAM-silencing group rAAV2/9 Syn-Flex-PSAM (L141F)GlyR-IRES-GFP (plasmid generous gift from S. Sternson, Janelia Farm; prepared by UPenn Vector Core); and (ii) for the GFP control group rAAV2/9 Syn-Flex-EGFP (B. Roth, University of North Carolina; prepared by UNC Vector Core). Imaging experiments in Fig. 4 used rAAV2/1 Syn-Flex-GCaMP6f (L. Looger, Janelia Farm; prepared by UPenn Vector Core). The following custom-prepared viruses were used for the LRIP activation and silencing experiments in Fig. 5, G to L and I to K, and Fig. 6, D to H: (i) rAAV2/7 Syn-Flex-Chr2-sfGFP; and (ii) rAAV2/7 Syn-Flex-PSAM-IRES-GFP [B. Zemelman, University of Texas at Austin (UT Austin), both custom-prepared]. Experiments in Fig. 6, A to E, involving (i) photostimulation of GABAergic CCK-Cre^+ INs used an rAAV2/7 Gad65-$(Chr2\text{-}sfGFP)^{Cre}$ (B. Zemelman, UT Austin, custom-prepared); (ii) photostimulation of PV-Cre^+ INs used rAAV2/5 EF1α-DIO-ChR2-EYFP [K. Deisseroth, Stanford University, commercially derived from UPenn (*58*)].

Surgery

Stereotaxic virus injection

The viral injection procedure is as previously described (*11*, *59*). Virus was injected into the brains of mice under stereotactic control by using thin glass pipettes pulled by using a micropipette puller and fire-polished with a microforge to have a long taper ending with a 10-μm tip diameter. Pipettes were first back-filled with light mineral oil, then front-filled with the virus by using a Nanoject II injector. Adult mice (5 to 10 weeks old) were injected with 50 μl buprenorphine (0.3 mg/ml), subsequently anesthetized with 3.5% isofluorane for 3 min (1.5 ml/min flow rate) in an induction chamber, head-fixed in a stereotaxic frame, and maintained under anesthesia with 1.5 to 2.5% isofluorane (1 ml/min) with a facemask. The hair on the head was clipped, the scalp sterilized with ethanol and betadine, and a 5- to 7-mm incision made to expose the skull.

The skull was then cleaned with hydrogen peroxide (0.1%), and the level adjusted to align bregma and lambda in the z axis. Small craniotomies were made bilaterally to target the dorsal hippocampal CA1 subfield [anteroposterior (A/P), −2.3 ± 0.2 from bregma; mediolateral

(M/L), 1.5 ± 0.2 from bregma, dorsoventral (D/V), −1.2 ± 0.2 mm from surface of the brain]; LEC (A/P, −3.2 ± 0.2 from bregma; M/L, 4.5 ± 0.2 from bregma, D/V, −2.5 ± 0.2 mm); and MEC (A/P 0.2 ± 0.2 from lamboid sinus at a 9° angle, M/L 3.1 ± 0.2 from lambda, D/V 0.9 ± 0.1 from surface of the brain). The pipette was lowered to penetrate the dura and a total of ~92 to 115 nl of virus was injected at each stereotactic coordinate (23 nl at a time with a 30-s interval between injections) by using the Nanoject II auto injector under slow mode. The pipette was retracted from the brain after a 5-min waiting period after the final injection per site. The scalp was disinfected with betadine, treated with triple antibiotic and the topical anesthetic Marcaine (0.5%), and sutured. Mice were allowed to recover for 2 to 4 weeks postinjection before the electrophysiology experiments.

Hippocampal cannula guide implantation

To selectively silence the long-range inhibitory projections from the entorhinal cortex to the hippocampus, we used local infusion of the cognate synthetic ligand PSEM in CA1 using a cannula. The presurgical and craniotomy procedures were identical to that of the stereotaxic viral injection. The skull surface was dried completely and coated with a thin layer of Vetbond and then lightly scratched with a scalpel blade to form crevices for the cement mix to seep in. A sterilized custom-designed bilateral cannula guide with a dummy cannula was inserted in the skull over dorsal hippocampal CA1 (A/P, −2.2; M/L, 1.5, D/V, −1.7 from bregma) along with two stainless steel anchoring screws inserted partially into the skull, one over the prefrontal cortex and the other over the cerebellum. The implant was secured to the animal's skull with dental cement (grip cement or dental acrylic) and two bone screws. The cement was allowed to dry for 20 min, and the wound was sutured around the implant. Marcaine was applied locally to decrease postoperative pain.

Hippocampal cranial window implantation

The cranial window implantation method used here is as described previously (*27*, *28*). The presurgical anesthesia and exposed skull preparation procedures were identical to that described above. A 3-mm-diameter circle was drilled in the skull over left dorsal CA1, to match the size of the cannula window implant. The bone and dura were gently removed, and the cortex covering the hippocampus was slowly aspirated while constant irrigation with chilled artificial cerebrospinal fluid (ACSF) was maintained until the external capsule was exposed. A sterilized stainless steel cannula implant with a glass cover slip window was inserted into the craniotomy. The top of the cannula and a titanium head post were secured to the skull with grip cement. The cement was allowed to dry for 20 min before mice were returned to the home cage.

Postsurgical care

The animals recovered from anesthesia and were mobile within 5 to 15 min postsurgery. Mice were monitored every 12 hours for 3 days after surgery, and buprenorphine was administered to minimize any signs of discomfort.

Freely moving behavior

The contextual fear conditioning and open-field behavioral tests were performed as described previously (*20*). The novel object recognition behavior task was a modified version of the paradigm described in (*25*) to ensure hippocampal dependence.

Subjects and habituation

Male mice (n = 4 or 5) were housed per cage with ad libitum access to food and water, kept on a 12-hour (6 a.m. to 6 p.m.) light-dark cycle with the ambient temperature maintained at 21°C. Tests were conducted during the light cycle. Half of the littermate mice in each cage were injected with the control GFP virus bilaterally in LEC, whereas the other half were injected with the PSAM virus. For 5 days before the start of behavioral testing, the mice were habituated to handling, transport from the postprocedural housing room to the behavioral testing room, and momentary head restraint for connecting the cannula guide with dummy tubing. During these habituation sessions, mice were allowed to move around with the tubing attached to simulate the PSEM infusion conditions. The experimenter was blind to the group identities, which were revealed after testing was completed.

Microinfusion of PSEM

An internal injection cannula was connected to a 10-µl Hamilton syringe via thin tubing. The tubing was prefilled with sterifiltered PSEM 308 (15 µM) in oxygen-enriched ACSF, and the syringe was mounted in a syringe pump. The animal was gently restrained in its home cage by hand, and the injection cannula was slowly introduced into the previously implanted guide cannula. The cannula was fixed to the head implant via a screw-top connector, and the animal was released in an empty cage. Next 0.5 µl of PSEM was injected over the course of 5 min with the syringe pump, followed by a 2-min rest period with the tubing connected to the animal. The animal was gently restrained once again by hand, the connector detached, the internal cannula removed, and the dummy internal cannula restored to the guide cannula. The animal was then placed in the open field, CFC chamber, or object recognition arena for testing in the behavioral tasks.

During all microinfusion experiments, the dye miniRuby (5% in water) was included in the cannula solution to gauge post hoc the accuracy of cannula targeting and spread of substances during the microinfusion. At the end of the experiments, the animals were infused with miniRuby again 10 min before perfusion with paraformaldehyde, and the brains were examined for miniRuby fluorescence. These experiments provide an overestimate of the likely extent of PSEM diffusion during its application, as the brains were analyzed 1 to 24 hours after the first miniRuby infusion and subjected to more than one miniRuby infusion, whereas PSEM is only active for 20 min after application (*19*)

Open field

Mice were placed in an open field (45 cm L by 45 cm W by 30.5 cm) for 30 min. The testing chambers were cleaned with 70% isopropanol wipes between animals to eliminate any odor-related cues. Locomotor and rearing activity was monitored via motion-sensitive infrared (IR) beam breaks and recorded by the Med Associates Activity Monitor software. The entire apparatus was enclosed in a soundproof box.

Contextual and cued fear conditioning

Hippocampus-dependent contextual fear memory and amygdala-dependent auditory fear memory were tested by using a 3-day-delay fear conditioning protocol. A sound-attenuating chamber equipped with a FireWire camera for tracking, a light, and a speaker for delivering contextual and conditioning cues was used. Mice were placed in an enclosure (17 cm by 17 cm by 25 cm) housed within the sound-attenuated chamber. The flooring, wall patterns, dominant odors, and light conditions of the enclosure could be changed to provide different contexts. Context A on day 1 consisted of an enclosure with a steel grid floor, three Plexiglas walls and one opaque wall with black and white stripes, 1% acetic acid as the dominant odor, and the house fan turned on. The enclosure was cleaned with 70% isopropanol between animals. Mice were moved from their home cage to a transfer cage with no bedding for the PSEM microinfusion as detailed above. After 2-min post-infusion of PSEM, the mice were placed in the fear conditioning chamber (context A). The mice explored the environment for 150 s, following which a tone (30 s, 2.8 kHz, 85 dB) was presented that coterminated with a shock (2 s, 0.7 mA). Mice were removed from the chamber 30 s after the shock. On day 2, the mice were placed back in context A for 300 s and contextual fear memory was assayed by scoring percent time spent freezing (defined as the absence of all movement except for respiration). No shock or tone was presented on day 2.

On day 3, the mice were exposed to novel context B: The testing room was dimly illuminated with red light, and the enclosure was cleaned between animals with Vimoba; the enclosure had an opaque white-colored plastic floor, with three solid gray-colored walls, one Plexiglas wall with a circular door, and a red, flat plastic roof and 0.25% benzaldehyde as the dominant odor. Mice were first moved from their home cage to a circular bucket and then a cage with paper towel bedding during PSEM infusion before moving them to the testing chamber. Mice were exposed to context B for 180 s, and then the tone from day 1 was played for 60 s to assess cued fear conditioning by using percentage of time spent freezing. Freezing during fear conditioning was analyzed automated with ANY-maze and parsed into the different behavioral task phases.

Novel object recognition

Twelve male mice were injected with AAV9-Syn-FLEX-PSAM L141F:GlyR-IRES-GFP (Penn)

Corrected 21 January 2016; see full text.

and kept on a 12-hour reversed light-dark cycle in a room maintained at 21°C. All trials of the novel object recognition (NOR) task were conducted during the dark cycle and in dim lighting. White plastic transport boxes (55 by 40 by 15 cm^3) were used as testing arenas. Three different objects were used: (i) a blue ceramic shoe (diameter 9.5 cm, maximal height 6 cm), (ii) a black plastic slide box (8 by 3 by 9.5 cm^3), and (iii) a semiclear plastic funnel (diameter 8.5 cm, maximal height 8.5 cm). Pilot experiments found that these objects elicited equal exploration time. Mice were habituated to handling and transported from the holding room to the behavioral room and were given 1 hour in the behavioral room each day to habituate before any tasks began. Mice were habituated to the infusion set-up and empty testing arena for 10 min each day for three consecutive days. On the fourth day, mice were infused over a duration of 5 min with either miniRuby + ACSF + PSEM or a control solution of miniRuby + ACSF. The solutions were kept in coded tubes to ensure that the experimenter was blinded and to randomize the treatment groups. In trial 1, mice were exposed to object A and object B for 10 min. After a 3-min intertrial interval, mice were again exposed to the same pair of objects for trial 2. The mice were then tested for object recognition memory after a 10-min interval by replacing either object A or object B with object C, the novel object. Objects and arenas were cleaned with 30% ethanol between all trials. Mice were recorded with an overhead FireWire camera and their movements tracked by using ANY-maze software. Exploration time was determined by using ANY-maze by measuring time spent with the animal's head within a region-of-interest (ROI) that extended 2 cm around each object.

In vivo imaging with head-fixed behavioral cues

Imaging experiments in head-fixed, awake behaving mice were performed as described previously (*27*, *28*). Briefly, Gad2-Cre: Ai14 tdTomato mice were injected in the left LEC with Cre-dependent rAAV to express the genetically encoded calcium indicator GCaMP6f (*26*) selectively in Cre^+ GABAergic neurons within the LEC. Two weeks postinjection, a glass-bottomed stainless steel cannula was implanted directly over the left hippocampus to allow for optical access to the long-range GABAergic axons projecting from LEC to SLM. After 1 week of recovery, water-deprived mice were head-fixed on a treadmill belt under a two-photon laser-scanning microscope within a custom-built behavioral apparatus that allows for simultaneous imaging and recording of behavior in response to four sensory stimuli: an aversive air puff to the snout, an appetitive water reward, a flash of light, and pure tones. Each experiment contained three to five blocks of stimuli presented either singularly or in pairs. Locomotion was monitored while imaging during each trial, which consisted of a 5- to 10-s pretrial interval, a randomly chosen stimulus or pair of stimuli, and a 10- to 30-s posttrial recording interval. Imaging was performed with an ultra fast pulsed laser beam (920-nm wavelength; 20 to 40 mW average power at the back focal plane of the objective) through a 40× objective. Green (GCaMP) and red (tdTomato) fluorescence was separated with an emission filter cube set (green, HQ525/70m-2p; red, HQ607/45m-2p; and 575dcxr) and was detected with photomultiplier tubes (PMTs) (green: GaAsP PMTs; red: multialkali PMTs) at either 256 × 128 pixels (75 × 75 μm; 0.295 μm/pixel in X; 0.588 μm/pixel in Y), 4× optical zoom, at 5.3 Hz or 128 × 128 pixels (105 × 105 μm), 2.8× optical zoon, at 6.1 Hz.

Acute-slice electrophysiology

Solutions

Recordings were performed with ACSF (pH 7.3, osmolarity 305 to 320 mOsm and saturated with 95% O_2 and 5% CO_2) for the extracellular solution. The ACSF consisted of (in mM) NaCl (125), $NaHCO_3$ (25), KCl (2.5), NaH_2PO_4 (1.25), $MgCl_2$ (1), $CaCl_2$ (2), glucose (22.5), Na-pyruvate (3), and ascorbate (1). Hippocampal slices were prepared and incubated in sucrose-enriched modified ACSF containing (in mM) NaCl (10), NaH_2PO_4 (1.2), KCl (2.5), $NaHCO_3$ (25), glucose (25), $CaCl_2$ (0.5), $MgCl_2$ (7), sucrose (190), and pyruvate (2). The intracellular current-clamp recording solution contained (in mM) $KMeSO_4$ (135), KCl (5), NaCl (2), EGTA (0.2), Hepes (10), phosphocreatine Na_2 (10), MgATP (5), Na_2GTP (0.4), Alexa Fluor 594 cadaverine (0.1), and biocytin (0.2%). The intracellular solution for voltage-clamp recordings contained $CsMeSO_4$ (135), KCl (5), NaCl (2), EGTA (0.2), Hepes (10), phosphocreatine Na_2 (10), MgATP (5), Na_2GTP (0.4), Alexa Fluor 594 (0.1), and biocytin (0.2%). In a subset of experiments, the following drugs were applied via bath application (in μM): SR95531 (2), CGP 55845 (1), NBQX (10), D-APV (100), and $PSEM^{308}$ (3 to 5). PSEM was generously provided by S. Sternson, Janelia Farm.

Slice preparation

We prepared 400-μm-thick horizontal hippocampal sections using a vibrating microtome from brains of mice that were transcardially perfused with ice-cold dissection ACSF. For the horizontal sections, hemisected brains were blocked ventromedially at an angle of 10° before sectioning. For the transverse sections, the hippocampi were dissected out, embedded in agar (4%), and then sliced. Slices were allowed to recover for at least 20 min at 34°C and then stored at room temperature in a 50% dissection: 50% standard ACSF solution before transfer to the recording chamber.

Electrophysiology setup

For IR-guided patch recordings, slices were visualized with a microscope equipped with Dodt-gradient-contrast optics and a 2× to 4× zoom module, IR filter, 60 × 1.0 nA water immersion objective, and a camera using image acquisition software. We performed fluorescence-guided targeted patch-clamp recordings using an epifluorescence illumination system equipped with a metal-halide lamp, ET-GFP and mCherry filter sets, Uniblitz shutter VCM-D1, and Orca R2 charge-coupled device camera controlled by μ-Manager (*60*). Photostimulation of ChR2 was achieved with an optical fiber coupled to a solid-state blue laser (470 nm) to illuminate SLM. In some experiments, the light was routed through a set of pinholes to produce a 50-μm focal-beam spot over SR.

Two-photon imaging and electrophysiology setup

Two-photon imaging of proximal dendritic spine Ca^{2+} used a custom-designed system with dual X-Y scanning galvanometers, coupled to a pulsed Ti:Sapphire MaiTai DeepSee femtosecond laser. Fluorescence was detected using high-sensitivity GaAsP PMTs. The scanning system was mounted on a microscope equipped with a 60 × 0.9 numerical aperture (NA) water immersion objective, and infrared Dodt-gradient-contrast optics coupled to a multialkali detector. Recording and stimulating electrodes were positioned using three junior micromanipulators on a movable motorized base plate connected to a MultiClamp 700B amplifier, Digidata 1440, and two constant-current stimulators for patch-clamp electrophysiology during imaging.

Electrophysiology recordings

Whole-cell patch-clamp recordings were performed at 34°C in standard ACSF using borosilicate glass pipettes with tip resistances of 3.5 to 4.5 MΩ for somatic and 9 to 16 MΩ for dendritic recordings. A MultiClamp 700B amplifier, pClamp 9 software, and a personal computer were used for data acquisition. Pipette capacitance (Cp), series resistance (Rs), and whole-cell capacitance (Cm) were compensated under voltage clamp initially with maximal allowable prediction and correction (75 to 85%). The average series resistance for whole-cell voltage-clamp recordings was kept between 9 and 15 MΩ. These values were used as a guide to estimate the pipette capacitance compensation and bridge balance under current clamp. The average access resistances for the current-clamp recordings ranged from 10 to 20 MΩ for soma and 10 to 40 MΩ for dendrite recordings. The membrane potential (V_m) of IN and pyramidal neuron soma was held at +10 mV under voltage clamp to measure IPSCs, whereas current clamp recordings were performed from soma and dendrites at the cell's resting membrane potential.

Synaptic responses were evoked by electrical stimulation of the EC inputs or SCs, with focal glass pipette stimulating electrodes coupled to constant current stimulators placed in SLM or SR, respectively. Stimulus strengths were adjusted to evoke EC and SC PSPs <50% of their maximal amplitude. Basal transmission was monitored every 15 s with EC and SC electrical stimuli spaced 2 s apart. Laser pulses delivered during episodes involving optical stimulation were also spaced 15 s apart. Cells were intracellularly filled for 10 to 15 min with the Ca^{2+} indicator Fluo-5F (500 μM) and the structural dye Alexa Fluor 594 (25 μM). Random-access line scans (256 lines per frame, 5.6× optical zoom, 25.709 × 17.504 μm field of vision, 2.8-μs dwell time, 1.28-ms scan-line period) and two-dimensional scan (512 × 512 pixels, 1× optical zoom, 198.45 × 198.45 μm field of vision,

1.6-μs dwell time, 1.4-ms scan-line period) image series were acquired using the PrairieView software in both the green and red channel. The image *t*-series acquisition on PrairieView was synchronized and used transistor-transistor logic triggered by the electrophysiology acquisition software Axograph. Line scans were acquired after each EC-SC stimulus pair simultaneously with the SC stimulus trigger once every 15 s for the single pairings at variable timing intervals (0 to 40 ms). For multiple pairings at 10- or 20-ms intervals, images were acquired at a 1 Hz frequency up to 90 times, identical to the ITDP induction protocol.

Immunohistochemistry, confocal imaging, and neuronal tracing

Immunohistochemistry

Adult animals were deeply anesthetized with ketamine-xylazine and perfused with 1× phosphate-buffered saline (PBS) followed by 4% parformaldehyde in PBS. The brains were removed and postfixed overnight in 4% paraformaldehyde at 4°C. The brains were sectioned in the coronal plane for hippocampal sections or sagittal plane for entorhinal sections at 50-μm thickness by using a vibrating microtome. For experiments involving the expression of GFP alone, GCaMP, and TdTomato, the signal was bright enough and did not require further immuno-enhancement. For immunostaining, slices were permeabilized in 1× PBS + 0.3% Triton, blocked in 3% normal goat serum, and then incubated with primary (overnight) and secondary (2 to 4 hours) antibodies in blocking solution (1× PBS, 0.2% Triton and 3% normal goat serum), unless otherwise stated. ChR2-EYFP– and ChR2-GFP–labeled neurons and their projections were stained by using a rabbit polyclonal antibody against GFP primary antibody (1:1000; Invitrogen) with a secondary goat antibody against primary rabbit immunoglobulin G (IgG) antibody conjugated with Alexa Fluor 488 dye (1:1000; Invitrogen). For the GFP-tagged CCK, PV, and SOM interneuron triple staining, we used a similar procedure for washing, permeabilization, and blocking as described above but substituted PBS with Tris-buffer solution (TBS, TB 0.1 M; NaCl 0.9%; pH 7.4). The primary antibodies we used were chicken polyclonal anti-GFP (1:1000, Abcam), rabbit polyclonal anti-parvalbumin (1:500, Synaptic Systems—SYSY), and rat monoclonal antibody against somatostatin (1:200, Millipore, clone YC7). The secondary antibodies for these stains included secondary goat antibody against chicken IgG antibody conjugated with Alexa Fluor 488 dye (1:1000, Invitrogen), goat anti-rabbit IgG antibody conjugated with Alexa Fluor 555 dye (1:1000, Invitrogen), and minimal cross reactivity goat anti-rat IgG conjugated with Alexa Fluor 647 dye (1:1000, Jackson Laboratories).

For experiments involving PSAM and CCK after electrophysiology recordings, 400-μm slices were drop-fixed overnight in 4% paraformaladhyde, embedded in agar, and resectioned to 50 μm. For the α-bungarotoxin staining of PSAM-GlyR, we followed the procedure previously described (*11*). Resliced sections were permeabilized with 0.5% Triton by using a Tris-buffered saline (TBS) at a pH of 7.4. The slices were blocked in 10% normal goat serum in TBS with 0.5% Triton for 4 hours at room temperature and then incubated with Alexa Fluor 647 α-bungarotoxin (1:3000; Invitrogen) in TBS + 0.1% Triton, first at room temperature for 1 hour, then at 4°C for 48 hours to stain for nicotinic α7 receptor–containing PSAM(L141F)-GlyR. In sections that coexpressed ChR2-GFP or GFP alone with the PSAM, primary antibody for GFP (rabbit polyclonal anti-GFP primary antibody, 1:1000; Invitrogen) was added for the last 12 hours of overnight incubation at 4°C. After TBS washes (4 × 15 min), the slices were incubated at room temperature for 4 hours with secondary antibody for GFP (goat antirabbit Alexa Fluor 488, 1:1000; Invitrogen) along with fresh Alexa Fluor 647 α-bungarotoxin (1:3000; Invitrogen) in TBS + 0.1% Triton to counterstain for GFP and PSAM. For the CCK staining, we followed a previously described procedure (*61*).

Briefly, slices were put through antigen retrieval by being placed in a citrate buffer at pH 8.6 for 70 min at 90°C. Then, slices were washed three times for 5 min each time in PBS. Slices were permeabilized with blocking solution (1% BSA and 0.5% Triton in PBS) with 10% normal goat serum for 4 hours at room temperature. Slices were then incubated with primary antibodies against cholecystokinin (mouse monoclonal; 1:1000; generous gift of G. Ohning, CURE center, UCLA) or GFP (rabbit polyclonal; 1:1000; Invitrogen) in blocking solution for 48 hours at 4°C. Slices were then washed 4 × 15 min each time with carrier solution (1% BSA, 0.1% Triton, and 1% normal goat serum in PBS) at room temperature. After this, slices were incubated with a Biotin-SP–conjugated AffiniPure $F(ab')_2$ fragment goat anti-mouse IgG (1:250; Jackson) and goat anti-rabbit Alexa Fluor 488 dye–conjugated IgG antibody (1:1000; Invitrogen) in carrier solution for 4 hours at room temperature. After PBS washes (4 × 15 min), the slices were incubated in ABC complex for 1 hour. Then slices were washed with PBS (4 × 15 min) and incubated with TSA-tyramide-tetramethylrhodamine amplification kit plus buffer solution for 3 to 10 min at room temperature. PBS washed slices were next incubated with Alexa Fluor 555 streptavidin (1:500; Invitrogen), Alexa Fluor 488 dye–conjugated anti-rabbit IgG secondary antibody (1:1000; Invitrogen), and Alexa Fluor 555 dye–conjugated anti-mouse IgG secondary antibody (1:1000; Invitrogen) in carrier solution for 4 hours at room temperature. Finally, the slices were washed in PBS (4 × 15 min) and mounted.

Stained slices were mounted with Prolong Gold or Vectashield hard-set mounting medium with 4′,6-diamidino-2-phenylindole (DAPI) for the GFP, CCK, PV, and somatostatin stains or Aqua-Mount aqueous mounting medium for the bungarotoxin staining.

Confocal imaging

An inverted laser-scanning confocal microscope was used to acquire tile scan and *Z*-stack images of multichannel fluorescent signals from fixed tissue sections by using 5×, 10×, or 20× air objectives, as well as a high NA 63× oil immersion objective. Maximum intensity projections were created using Image J.

Neuronal reconstruction

During the electrophysiology recordings, all cells were intracellularly filled with Alexa Fluor 594 for online visualization and 0.2% neurobiotin to allow for enhanced visualization and post hoc reconstruction with a streptavidin-bound fluorophore (Streptavidin Alexa Fluor 555). Immediately after recording, the acute brain slice was drop-fixed overnight at 4°C in 4% paraformaldehyde solution. The tissue was then thoroughly rinsed with PBS-glycine (1 × 15 min) and PBS (3 × 15 min) and processed for immunohistochemistry. The 20× high-resolution (1024 × 1024, 16-bit depth) fluorescent confocal *Z*-stack images of the fluorophore-labeled filled neurons were used to trace the soma, axons, and dendrites by using Neurolucida reconstruction software.

Data analysis

Behavior data

For the behavioral experiments, we analyzed the open-field data using Activity Monitor, and an automated analysis was used for calculating freezing during fear conditioning with ANY-maze. The data were exported in tab-delimited format into Prism for further statistical analysis. The red fluorescent signal of miniRuby infused along with PSEM during the behavioral tasks served as an indicator of accurate cannula targeting and drug spread. One animal from the control cohort (total of 10 animals) and test cohort (total of 8 animals) each was removed from the data analysis because of mistargeting. Statistical significance was assessed by two-tailed unpaired Student's *t* tests, two-way ANOVA, or two-way repeated-measures ANOVA where appropriate. Significant main effects or interactions were followed up with multiple comparison testing by using Sidak's correction. Results were considered significant when $P < 0.05$. α was set equal to 0.05 for multiple comparison tests. Sample sizes were chosen based on previous studies.

In vivo imaging data

Sequential Image Analysis (SIMA) toolkit (*62*) was used to correct motion artifacts in the raw imaging data, to identify and tag regions of interest (ROIs), and to extract fluorescence traces from each ROI. Extracted signals were synchronized to the recorded running signal and presented stimuli, and peristimulus time histograms (PSTHs) were calculated. For each ROI-stimulus pair, the response magnitude was calculated as the mean of the PSTH in the 3 s preceding the stimulus subtracted from the mean of the 3 s after the stimulus. Significantly responding ROIs were determined by randomly shuffling the stimulus times across all trials 10,000 times, calculating the response magnitude for each shuffle, and then selecting any ROIs with a response magnitude

Corrected 21 January 2016; see full text.

above the 95th percentile of the distribution of shuffled values.

Electrophysiology data

Axograph X was used for electrophysiology data analysis. A 7pA amplitude threshold was set for sorting failures and successes for the light-evoked IPSCs to map the LEC and MEC LRIP connectivity. All IPSCs above this cutoff were included in calculating the mean response amplitude and percentage of responsive INs for the two groups. For calculating amplitude changes in the EC-SC and EC-ChR2 single pairing, the responses to SC electrical stimulation or ChR2 photostimulation alone were averaged for 3 min before pairing, and the mean was used to normalize the responses paired with EC stimulation. For comparing the effect of application of NBQX, APV, SR 95531, CGP 55845, or PSEM, the predrug baseline synaptic-response amplitude for the "control" condition was obtained by averaging the responses recorded for the 5 min preceding drug application. The postdrug synaptic-response amplitudes were obtained by averaging responses recorded for 5 min in the presence of the drug, once a steady-state response was reached, typically 7 to 10 min after starting bath application of the drug. For sorting and generating the histograms of the dendritic PSPs and spikes, an event-detection algorithm in Axograph was used. Time-course plots for ITDP were generated by using a boxcar average of every four responses (1-min period), as previously described (*11*). All statistical errors are standard errors of the population mean or boxcar mean (SEM); all P values (significance level set at $P < 0.05$) for t tests are two-tailed; and all ANOVAs were corrected for multiple comparisons using post hoc tests as indicated.

KaleidaGraph 4 and Prism 6 were used for plotting all data and statistical analysis. Figures were generated with Adobe Illustrator.

REFERENCES AND NOTES

1. V. H. Brun *et al*., Impaired spatial representation in CA1 after lesion of direct input from entorhinal cortex. *Neuron* **57**, 290–302 (2008). doi: 10.1016/j.neuron.2007.11.034; pmid: 18215625
2. J. Suh, A. J. Rivest, T. Nakashiba, T. Tominaga, S. Tonegawa, Entorhinal cortex layer III input to the hippocampus is crucial for temporal association memory. *Science* **334**, 1415–1420 (2011). doi: 10.1126/science.1210125; pmid: 22052975
3. T. Kitamura *et al*., Island cells control temporal association memory. *Science* **343**, 896–901 (2014). doi: 10.1126/science.1244634; pmid: 24457215
4. S. Melzer *et al*., Long-range-projecting GABAergic neurons modulate inhibition in hippocampus and entorhinal cortex. *Science* **335**, 1506–1510 (2012). doi: 10.1126/science.1217139; pmid: 22442486
5. D. G. Amaral, M. P. Witter, The three-dimensional organization of the hippocampal formation: A review of anatomical data. *Neuroscience* **31**, 571–591 (1989). doi: 10.1016/0306-4522(89)90424-7; pmid: 2687721
6. M. P. Witter, D. G. Amaral, Entorhinal cortex of the monkey: V. Projections to the dentate gyrus, hippocampus, and subicular complex. *J. Comp. Neurol.* **307**, 437–459 (1991). doi: 10.1002/cne.903070308; pmid: 1713237
7. G. Buzsáki, Feed-forward inhibition in the hippocampal formation. *Prog. Neurobiol.* **22**, 131–153 (1984). doi: 10.1016/0301-0082(84)90023-6; pmid: 6433403
8. T. Jarsky, A. Roxin, W. L. Kath, N. Spruston, Conditional dendritic spike propagation following distal synaptic activation of hippocampal CA1 pyramidal neurons. *Nat. Neurosci.* **8**, 1667–1676 (2005). doi: 10.1038/nn1599; pmid: 16299501
9. H. Takahashi, J. C. Magee, Pathway interactions and synaptic plasticity in the dendritic tuft regions of CA1 pyramidal neurons. *Neuron* **62**, 102–111 (2009). doi: 10.1016/j.neuron.2009.03.007; pmid: 19376070
10. J. T. Dudman, D. Tsay, S. A. Siegelbaum, A role for synaptic inputs at distal dendrites: Instructive signals for hippocampal long-term plasticity. *Neuron* **56**, 866–879 (2007). doi: 10.1016/j.neuron.2007.10.020; pmid: 18054862
11. J. Basu *et al*., A cortico-hippocampal learning rule shapes inhibitory microcircuit activity to enhance hippocampal information flow. *Neuron* **79**, 1208–1221 (2013). doi: 10.1016/j.neuron.2013.07.001; pmid: 24050406
12. K. C. Bittner *et al*., Conjunctive input processing drives feature selectivity in hippocampal CA1 neurons. *Nat. Neurosci.* **18**, 1133–1142 (2015). doi: 10.1038/nn.4062; pmid: 26167906
13. V. H. Brun *et al*., Place cells and place recognition maintained by direct entorhinal-hippocampal circuitry. *Science* **296**, 2243–2246 (2002). doi: 10.1126/science.1071089 pmid: 12077421
14. M. Fyhn, S. Molden, M. P. Witter, E. I. Moser, M. B. Moser, Spatial representation in the entorhinal cortex. *Science* **305**, 1258–1264 (2004). doi: 10.1126/science.1099901; pmid: 15333832
15. E. L. Hargreaves, G. Rao, I. Lee, J. J. Knierim, Major dissociation between medial and lateral entorhinal input to dorsal hippocampus. *Science* **308**, 1792–1794 (2005). doi: 10.1126/science.1110449; pmid: 15961670
16. H. Taniguchi *et al*., A resource of Cre driver lines for genetic targeting of GABAergic neurons in cerebral cortex. *Neuron* **71**, 995–1013 (2011). doi: 10.1016/j.neuron.2011.07.026; pmid: 21943598
17. E. S. Boyden, F. Zhang, E. Bamberg, G. Nagel, K. Deisseroth, Millisecond-timescale, genetically targeted optical control of neural activity. *Nat. Neurosci.* **8**, 1263–1268 (2005). doi: 10.1038/nn1525; pmid: 16116447
18. S. Maren, K. L. Phan, I. Liberzon, The contextual brain: Implications for fear conditioning, extinction and psychopathology. *Nat. Rev. Neurosci.* **14**, 417–428 (2013). doi: 10.1038/nrn3492; pmid: 23635870
19. C. J. Magnus *et al*., Chemical and genetic engineering of selective ion channel-ligand interactions. *Science* **333**, 1292–1296 (2011). doi: 10.1126/science.1206606; pmid: 21885782
20. F. L. Hitti, S. A. Siegelbaum, The hippocampal CA2 region is essential for social memory. *Nature* **508**, 88–92 (2014). doi: 10.1038/nature13028; pmid: 24572357
21. S. J. Cohen, R. W. Stackman Jr., Assessing rodent hippocampal involvement in the novel object recognition task. A review. *Behav. Brain Res.* **285**, 105–117 (2015). doi: 10.1016/j.bbr.2014.08.002; pmid: 25169255
22. R. E. Clark, S. M. Zola, L. R. Squire, Impaired recognition memory in rats after damage to the hippocampus. *J. Neurosci.* **20**, 8853–8860 (2000). pmid: 11102494
23. J. A. Ainge *et al*., The role of the hippocampus in object recognition in rats: Examination of the influence of task parameters and lesion size. *Behav. Brain Res.* **167**, 183–195 (2006). doi: 10.1016/j.bbr.2005.09.005; pmid: 16214239
24. S. J. Cohen *et al*., The rodent hippocampus is essential for nonspatial object memory. *Curr. Biol.* **23**, 1685–1690 (2013). doi: 10.1016/j.cub.2013.07.002; pmid: 23954431
25. C. A. Denny, N. S. Burghardt, D. M. Schachter, R. Hen, M. R. Drew, 4- to 6-week-old adult-born hippocampal neurons influence novelty-evoked exploration and contextual fear conditioning. *Hippocampus* **22**, 1188–1201 (2012). doi: 10.1002/hipo.20964; pmid: 21739523
26. T. W. Chen *et al*., Ultrasensitive fluorescent proteins for imaging neuronal activity. *Nature* **499**, 295–300 (2013). doi: 10.1038/nature12354; pmid: 23868258
27. P. Kaifosh, M. Lovett-Barron, G. F. Turi, T. R. Reardon, A. Losonczy, Septo-hippocampal GABAergic signaling across multiple modalities in awake mice. *Nat. Neurosci.* **16**, 1182–1184 (2013). doi: 10.1038/nn.3482; pmid: 23912949
28. M. Lovett-Barron *et al*., Dendritic inhibition in the hippocampus supports fear learning. *Science* **343**, 857–863 (2014). doi: 10.1126/science.1247485; pmid: 24558155
29. D. W. Cope *et al*., Cholecystokinin-immunopositive basket and Schaffer collateral-associated interneurones target different domains of pyramidal cells in the CA1 area of the rat hippocampus. *Neuroscience* **109**, 63–80 (2002). doi: 10.1016/S0306-4522(01)00440-7; pmid: 11784700
30. T. Klausberger, P. Somogyi, Neuronal diversity and temporal dynamics: The unity of hippocampal circuit operations. *Science* **321**, 53–57 (2008). doi: 10.1126/science.1149381; pmid: 18599766
31. H. Pawelzik, D. I. Hughes, A. M. Thomson, Physiological and morphological diversity of immunocytochemically defined parvalbumin- and cholecystokinin-positive interneurones in CA1 of the adult rat hippocampus. *J. Comp. Neurol.* **443**, 346–367 (2002). doi: 10.1002/cne.10118; pmid: 11807843
32. S. H. Lee, I. Soltesz, Requirement for CB1 but not GABAB receptors in the cholecystokinin mediated inhibition of GABA release from cholecystokinin expressing basket cells. *J. Physiol.* **589**, 891–902 (2011). doi: 10.1113/jphysiol.2010.198499; pmid: 21173082
33. M. I. Daw, L. Tricoire, F. Erdelyi, G. Szabo, C. J. McBain, Asynchronous transmitter release from cholecystokinin-containing inhibitory interneurons is widespread and target-cell independent. *J. Neurosci.* **29**, 11112–11122 (2009). doi: 10.1523/JNEUROSCI.5760-08.2009; pmid: 19741117
34. N. L. Golding, N. P. Staff, N. Spruston, Dendritic spikes as a mechanism for cooperative long-term potentiation. *Nature* **418**, 326–331 (2002). doi: 10.1038/nature00854; pmid: 12124625
35. F. Gambino *et al*., Sensory-evoked LTP driven by dendritic plateau potentials in vivo. *Nature* **515**, 116–119 (2014). doi: 10.1038/nature13664; pmid: 25174710
36. N. L. Golding, N. Spruston, Dendritic sodium spikes are variable triggers of axonal action potentials in hippocampal CA1 pyramidal neurons. *Neuron* **21**, 1189–1200 (1998). doi: 10.1016/S0896-6273(00)80635-2; pmid: 9856473
37. M. E. Larkum, J. J. Zhu, B. Sakmann, A new cellular mechanism for coupling inputs arriving at different cortical layers. *Nature* **398**, 338–341 (1999). doi: 10.1038/18686; pmid: 10192334
38. G. Buzsáki, E. I. Moser, Memory, navigation and theta rhythm in the hippocampal-entorhinal system. *Nat. Neurosci.* **16**, 130–138 (2013). doi: 10.1038/nn.3304; pmid: 23354386
39. A. Kamondi, L. Acsády, G. Buzsáki, Dendritic spikes are enhanced by cooperative network activity in the intact hippocampus. *J. Neurosci.* **18**, 3919–3928 (1998). pmid: 9570819
40. A. Losonczy, J. K. Makara, J. C. Magee, Compartmentalized dendritic plasticity and input feature storage in neurons. *Nature* **452**, 436–441 (2008). doi: 10.1038/nature06725; pmid: 18368112
41. M. E. Sheffield, D. A. Dombeck, Calcium transient prevalence across the dendritic arbour predicts place field properties. *Nature* **517**, 200–204 (2015). doi: 10.1038/nature13871; pmid: 25363782
42. S. Royer *et al*., Control of timing, rate and bursts of hippocampal place cells by dendritic and somatic inhibition. *Nat. Neurosci.* **15**, 769–775 (2012). doi: 10.1038/nn.3077; pmid: 22446878
43. L. Roux, G. Buzsáki, Tasks for inhibitory interneurons in intact brain circuits. *Neuropharmacology* **88**, 10–23 (2015). doi: 10.1016/j.neuropharm.2014.09.011; pmid: 25239808
44. A. J. Murray *et al*., Parvalbumin-positive CA1 interneurons are required for spatial working but not for reference memory. *Nat. Neurosci.* **14**, 297–299 (2011). doi: 10.1038/nn.2751; pmid: 21278730
45. F. Donato, S. B. Rompani, P. Caroni, Parvalbumin-expressing basket-cell network plasticity induced by experience regulates adult learning. *Nature* **504**, 272–276 (2013). doi: 10.1038/nature12866; pmid: 24336286
46. S. Hefft, P. Jonas, Asynchronous GABA release generates long-lasting inhibition at a hippocampal interneuron-principal neuron synapse. *Nat. Neurosci.* **8**, 1319–1328 (2005). doi: 10.1038/nn1542; pmid: 16158066
47. T. Klausberger *et al*., Complementary roles of cholecystokinin- and parvalbumin-expressing GABAergic neurons in hippocampal network oscillations. *J. Neurosci.* **25**, 9782–9793 (2005). doi: 10.1523/JNEUROSCI.3269-05.2005 pmid: 16237182
48. W. Jacob, R. Marsch, G. Marsicano, B. Lutz, C. T. Wotjak, Cannabinoid CB1 receptor deficiency increases contextual fear memory under highly aversive conditions and long-term potentiation in vivo. *Neurobiol. Learn. Mem.* **98**, 47–55 (2012). doi: 10.1016/j.nlm.2012.04.008; pmid: 22579951
49. M. F. Yeckel, T. W. Berger, Feedforward excitation of the hippocampus by afferents from the entorhinal cortex: Redefinition of the role of the trisynaptic pathway. *Proc. Natl. Acad. Sci. U.S.A.* **87**, 5832–5836 (1990). doi: 10.1073/pnas.87.15.5832; pmid: 2377621
50. E. W. Schomburg *et al*., Theta phase segregation of input-specific gamma patterns in entorhinal-hippocampal networks. *Neuron* **84**, 470–485 (2014). doi: 10.1016/j.neuron.2014.08.051; pmid: 25263753
51. J. J. Chrobak, A. Lörincz, G. Buzsáki, Physiological patterns in the hippocampo-entorhinal cortex system. *Hippocampus* **10**, 457–465 (2000). doi: 10.1002/1098-1063(2000)10:4<457::AID-HIPO12>3.0.CO;2-Z; pmid: 10985285

52. K. M. Igarashi, L. Lu, L. L. Colgin, M. B. Moser, E. I. Moser, Coordination of entorhinal-hippocampal ensemble activity during associative learning. *Nature* **510**, 143–147 (2014). doi: 10.1038/nature13162; pmid: 24739966
53. T. Nakashiba, J. Z. Young, T. J. McHugh, D. L. Buhl, S. Tonegawa, Transgenic inhibition of synaptic transmission reveals role of CA3 output in hippocampal learning. *Science* **319**, 1260–1264 (2008). doi: 10.1126/science.1151120; pmid: 18218862
54. S. Hippenmeyer *et al*., A developmental switch in the response of DRG neurons to ETS transcription factor signaling. *PLOS Biol.* **3**, e159 (2005). doi: 10.1371/journal.pbio.0030159; pmid: 15836427
55. L. Madisen *et al*., A robust and high-throughput Cre reporting and characterization system for the whole mouse brain. *Nat. Neurosci.* **13**, 133–140 (2010). doi: 10.1038/nn.2467; pmid: 20023653
56. G. Miyoshi *et al*., Genetic fate mapping reveals that the caudal ganglionic eminence produces a large and diverse population of superficial cortical interneurons. *J. Neurosci.* **30**, 1582–1594 (2010). doi: 10.1523/JNEUROSCI.4515-09.2010; pmid: 20130169
57. M. Yamamoto *et al*., A multifunctional reporter mouse line for Cre- and FLP-dependent lineage analysis. *Genesis* **47**, 107–114 (2009). doi: 10.1002/dvg.20474; pmid: 19165827
58. F. Zhang *et al*., Optogenetic interrogation of neural circuits: Technology for probing mammalian brain structures. *Nat. Protoc.* **5**, 439–456 (2010). doi: 10.1038/nprot.2009.226; pmid: 20203662
59. J. V. Kupferman *et al*., Reelin signaling specifies the molecular identity of the pyramidal neuron distal dendritic compartment. *Cell* **158**, 1335–1347 (2014). doi: 10.1016/j.cell.2014.07.035; pmid: 25201528
60. A. Edelstein, N. Amodaj, K. Hoover, R. Vale, N. Stuurman, Computer control of microscopes using μManager. *Curr. Protoc. Mol. Biol.* Chap.: Unit 14.20 (2010). pmid: 20890901
61. L. Tricoire *et al*., A blueprint for the spatiotemporal origins of mouse hippocampal interneuron diversity. *J. Neurosci.* **31**, 10948–10970 (2011). doi: 10.1523/JNEUROSCI.0323-11.2011; pmid: 21795545
62. P. Kaifosh, J. D. Zaremba, N. B. Danielson, A. Losonczy, SIMA: Python software for analysis of dynamic fluorescence imaging data. *Front. Neuroinform.* **8**, 80 (2014). doi: 10.3389/fninf.2014.00080

ACKNOWLEDGMENTS

We thank K. Deisseroth, S. Sternson, Z. J. Huang, and G. Fishell for generously sharing reagents and transgenic mice. We thank V. Jayaraman, R. A. Kerr, D. S. Kim, L. L. Looger, and K. Svoboda from the GENIE Project, Janelia Farm Research Campus, Howard Hughes Medical Institute, for the use of the GCaMP6f-encoding virus. We are grateful to G. Buzsaki, R. Tsien, R. Hen, Al. Dranovsky, C. Kellendonk, S. Fusi, R. Bruno, and A. Das for invaluable discussions on the study and C. Magnus, S. Sternson, C. Denny, A. Katzman, and M. Russo for critical technical advice. We are also indebted to J. Kupferman, Z. Rosen, A. Masurkar, Q. Sun, and T. Bock for helpful comments on previous versions of the manuscript. This work was supported by a NARSAD Young Investigator grant to J.B.; a Ruth L. Kirschstein F30 National Research Service Award from the National Institute of Mental Health (NIMH), NIH, to F.L.H.; a Human Frontier Science Program grant and a grant (1R01MH100510) from NIMH to B.V.Z.; a grant (1R01MH100631) from NIMH and support from the Searle Scholars Program, Human Frontier Science Program, and the McKnight Memory and Cognitive Disorders Award to A.L.; and a grant (R01NS036658) from National Institute of Neurological Disorders and Stroke, NIH, and support from the Howard Hughes Medical Institute to S.A.S.

SUPPLEMENTARY MATERIALS

www.sciencemag.org/content/351/6269/aaa5694/suppl/DC1
Figs. S1 to S10
References (*63*–*67*)
Movie S1

24 December 2014; accepted 17 November 2015
10.1126/science.aaa5694

Gating of hippocampal activity, plasticity, and memory by entorhinal cortex long-range inhibition

Jayeeta Basu, Jeffrey D. Zaremba, Stephanie K. Cheung, Frederick L. Hitti, Boris V. Zemelman, Attila Losonczy and Steven A. Siegelbaum (January 7, 2016)

Science **351** (6269), . [doi: 10.1126/science.aaa5694]

Editor's Summary

Fine-tuned information flow in the brain

In addition to providing well-characterized excitatory inputs, the entorhinal cortex also sends long-range inhibitory projections to the hippocampus. Basu *et al.* described this input in detail and characterized its role for learning and memory. Multimodal sensory stimuli activate long-range inhibitory input in vivo. This input enables precisely timed information transfer within the cortico-hippocampal circuit. In this way, long-range inhibitory projections play an important role in providing specificity of fear conditioning, and thus help prevent overgeneralization.

Science, this issue p. 10.1126/science.aaa5694